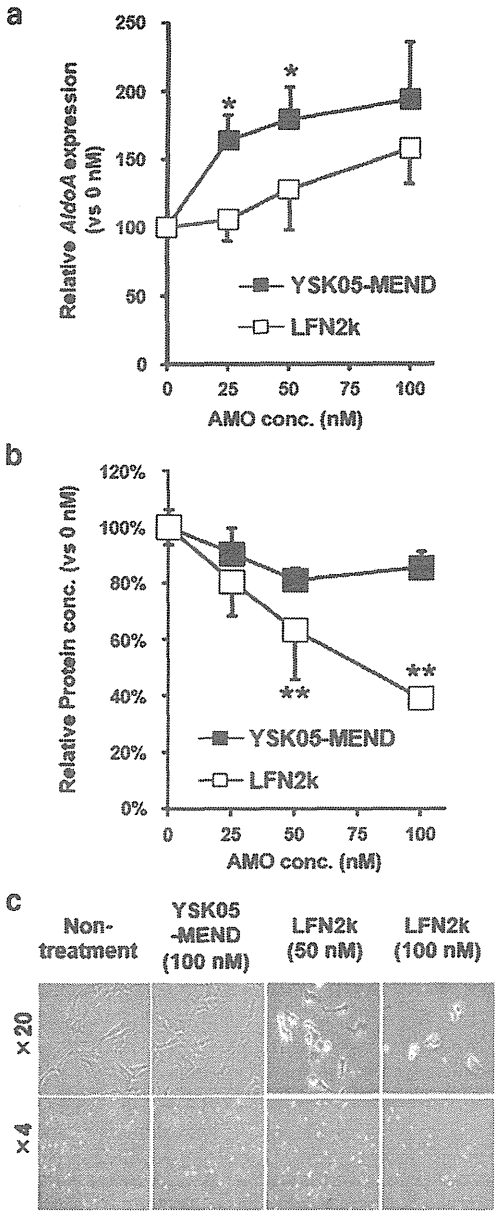

Fig. 1. Expression of miR-122 and *AldoA* and cytotoxicity *in vitro*. (a) The expression of *AldoA* in Hepa1c1c7 cells treated with YSK05-MEND or LFN2k at the indicated AMO122 concentrations was evaluated by qRT-PCR. The expression of *AldoA* was normalized to *Hprt1*. Data are represented as relative expression levels to that treated with PBS (0 nM). The mean ± SD (n = 3). (b) Protein levels were determined after treatment with YSK05-MEND or LFN2k. Data are represented relative values to that treated with PBS (0 nM). The Mean ± SD (n = 3). *P < 0.05, **P < 0.01 YSK05-MEND v.s. LFN2k at indicated AMO concentrations.

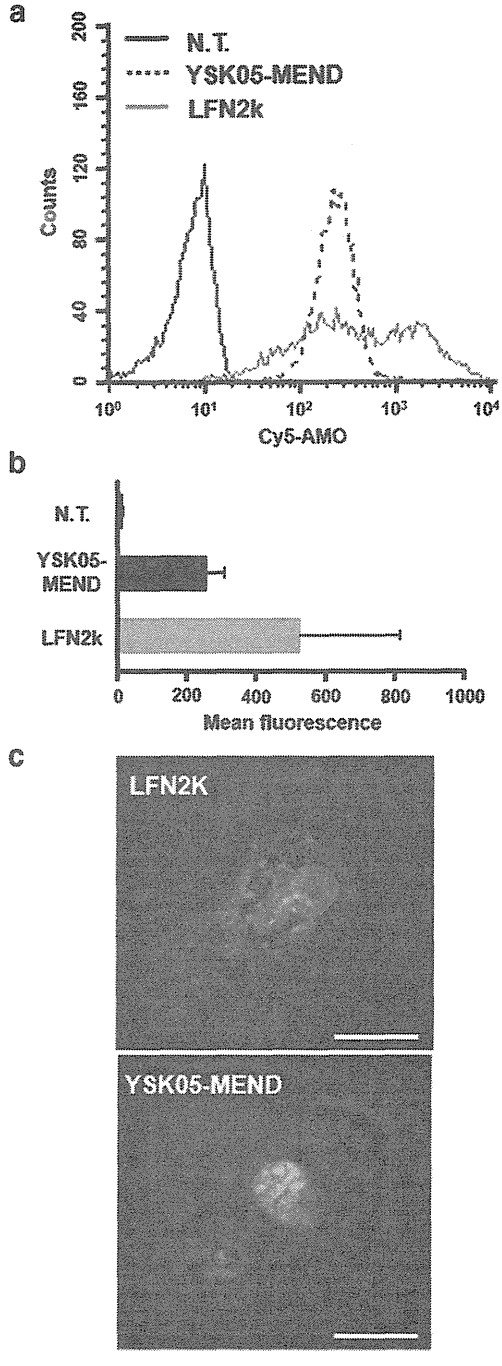

Fig. 2. Cellular uptake and intracellular distribution of Cy5-AMO. (a) The uptake of Cy5-AMO formulated in the YSK05-MEND and LFN2k were determined by a flow cytometry, after a 2 h incubation at 20 nM AMO. (b) Bars represent average fluorescence obtained by flow cytometric analysis (n = 3). N.T.: Non-treatment. (c) The intracellular pattern of Cy5-AMO (red) formulated in YSK05-MEND and LFN2k was observed by a confocal laser scanning microscope after the incubation for 2 h at 80 nM AMO. Nuclei were stained with Hoechst 33342 prior to observation (cyan). Scale bars indicate 20 μm.

3.3. *In vivo evaluation of AMO encapsulated YSK05-MEND*

We next evaluated the *in vivo* efficacy of the AMO122-YSK05-MEND in the liver. It is known that LFN2k cannot be used *in vivo*, and therefore, chemically modified anti-miRs are largely administered as a free form in *in vivo* studies [3,4,12–14]. Therefore, we used free AMO122 as a control in the *in vivo* studies. To observe the distribution of AMOs, mice were administered with the YSK05-MEND encapsulating Cy5-AMO *via* the tail vein. After 30 min, nuclear stained liver sections were prepared and observed by confocal laser scanning microscopy. As shown in Fig. 3, the administration of the YSK05-MEND resulted in a higher fluorescent signal of Cy5-AMO in the liver as compared to that of free Cy5-AMO. Conversely, the free Cy5-AMO accumulated at higher levels

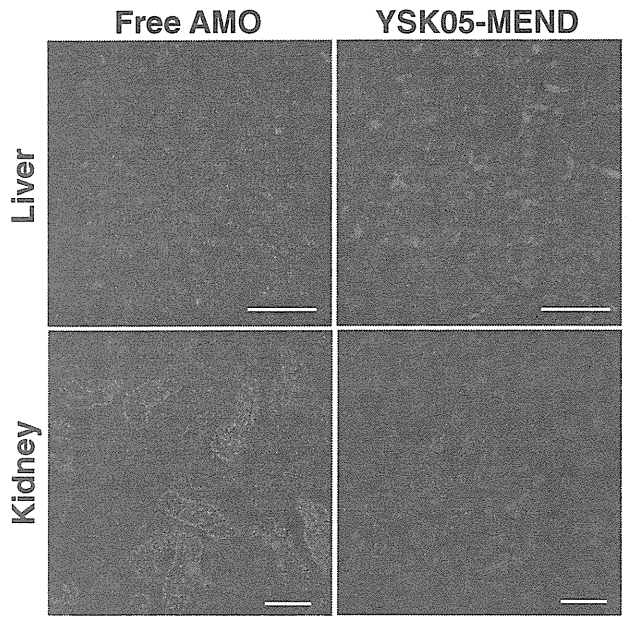

Fig. 3. Histological observations of Cy5-AMO in the liver and kidney. Mice were injected *via* the tail vein with either free Cy5-AMO or Cy5-AMO encapsulated in the YSK05-MEND (red). The liver and kidney were collected 30 min later. Nuclei in the liver and kidney were stained with Hoechst33342 (blue). Images were captured by a CLSM. Scale bars are 50 μm.

in the kidney than the YSK05-MEND because the free Cy5-AMO was excreted *via* the kidney due to its molecular weight.

We evaluated the knockdown of miR-122 in the liver. Either free AMO122, AMO122-YSK05-MEND or empty YSK05-MEND was successively administered three times at a dose of 1 mg AMO122/kg. Even though the administration of free AMO122 resulted in an approximately 30% knockdown of miR-122, the AMO122-YSK05-MEND significantly reduced the expression of miR-122 as compared to free AMO122 as well as the empty YSK05-MEND at 48 h after the last administration (day 6) (Fig. 4a). The expression levels of genes that are regulated by miR-122 were determined. YSK05-MEND enhanced the expression of *AldoA*, *Bckdk* and *Ndrg3*, while no increase in the expression of these genes was found in the case of free AMO122 (Fig. 4b). These alternations were not observed when YSK05-MEND encapsulating AMO against miR-10b (AMO10b) was used (Fig. S2). It was reported that miR-122 is a key regulator of cholesterol, and the inhibition of miR-122 resulted in a decrease in plasma cholesterol levels [3,4]. Hence, plasma cholesterol levels were measured. Plasma cholesterol levels were decreased by around 30% only by treatment with the AMO122-YSK05-MEND at 48 h after the last injection (day 6) (Fig. 4c).

We further monitored the expression of miR-122 and its target genes at days 6, 12 and 25, as well as plasma cholesterol levels until day 25 after the AMO122-YSK05-MEND treatment and compared the findings to that of PBS to estimate the durability of AMO122-YSK05-MEND. The knockdown of miR-122 and enhancement of the genes by AMO122-YSK05-MEND continued until day 12 (Fig. 5a and d). The significant decline in plasma cholesterol levels continued until day 18 compared to the control that was treated with PBS (Fig. 5c). On the other hand, no significant difference in body weight was observed over the 25 days (Fig. 5d). Because liposomal systems mainly accumulate in the liver, hepatotoxicity was evaluated. The findings showed that no increase in serum ALT levels occurred at 48 h after the last injection of AMO122-YSK05-MEND (Fig. 5e).

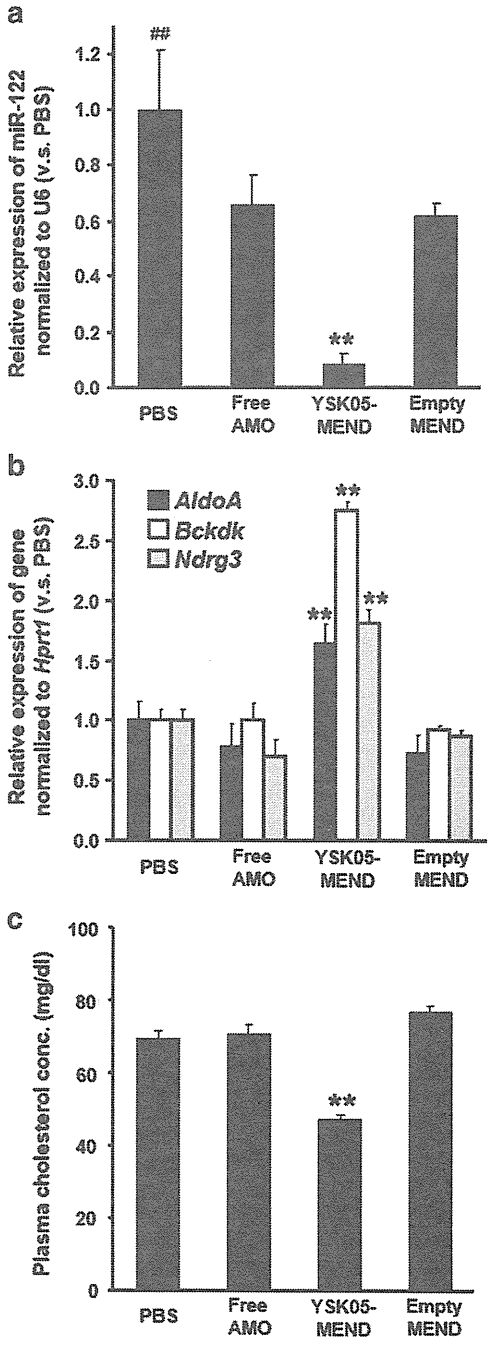

Fig. 4. Expression of miR-122 and target genes in the liver and cholesterol levels in plasma. Mice were injected at days 0, 2 and 4 *via* the tail vein with either PBS, free AMO122 (1 mg AMO/kg), AMO122-YSK05-MEND (1 mg AMO/kg) or empty YSK05-MEND. At 48 h after the last injection (day 6), the expression of (a) miR-122 and (b) *AldoA*, *Bckdk* and *Ndrg3* in the liver and (c) plasma cholesterol level were determined (the mean ± SD, n = 4). $^{**}P < 0.01$ YSK05-MEND v.s. the others. $^{\#\#}P < 0.01$ PBS v.s. the others.

4. Discussion

MiRNAs have emerged as important post-transcriptional regulators of gene expression in biological processes [1]. Loss of function studies using miRNA gene knockout techniques are frequently utilized to explore the functions of miRNAs [11,29]. However, the generation of

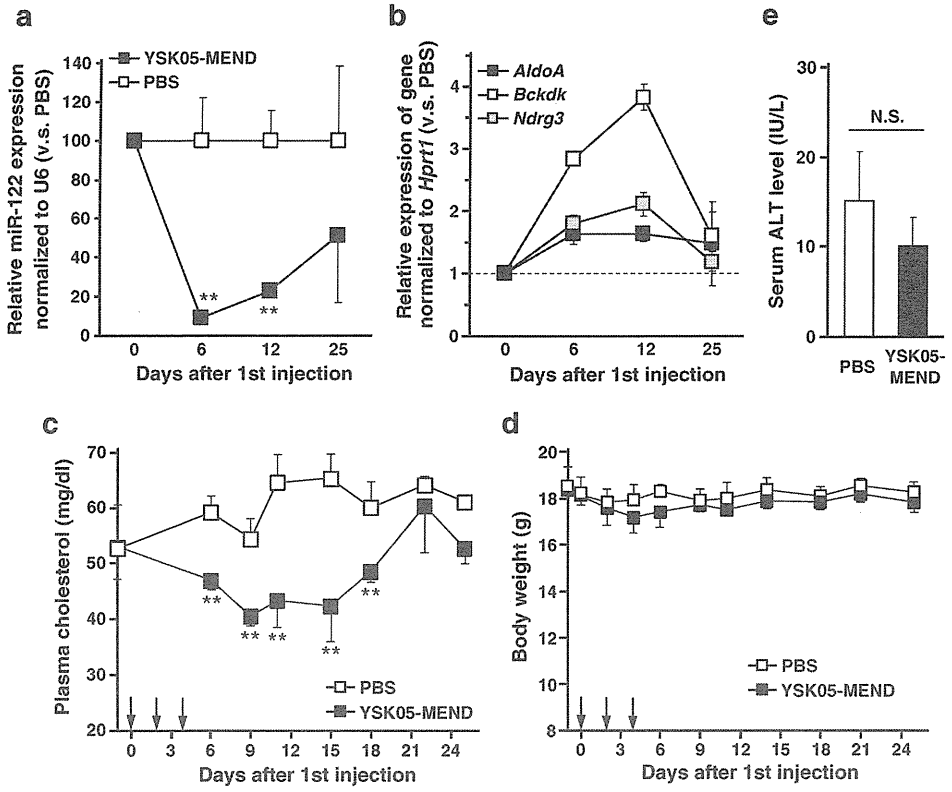

Fig. 5. Long-term observation of the expression level of miR-122 and target genes in the liver and plasma cholesterol levels. Mice were injected *via* the tail vein with either PBS or AMO122-YSK05-MEND at days 0, 2 and 4. (a, b) The expression of miR-122 (a) and target genes (b) in liver was determined at days 6, 12 and 25. (c, d) The cholesterol level in plasma (c) and body weight (d) were monitored over 25 days. Arrows indicate the injections at days 0, 2 and 4. (e) Serum ALT was determined at day 6. Data are represented as the mean ± SD (n = 4). **P < 0.01 v.s. PBS-treatment at indicated time points. N.S.: Not significant difference.

genetic knockouts is difficult, complicating and time consuming. A widely employed approach in loss-of-function studies is to use chemically modified anti-miRs [3–5,12–14], and LNA-modified anti-miR has some potential for clinical use in the treatment of HCV infections [15]. For a successful anti-miRNA therapy using anti-miRs, the anti-miRs must be delivered to the final destination, *i.e.* the cytoplasm of the target cell. Even though a variety of chemical modifications have been reported to improve nuclease resistance and binding affinity to miRNAs, the delivery of anti-miRs to target organs and the cytoplasm in target cells continues to be a significant challenge. Significant efforts have been devoted to exploring novel delivery strategies, and liposomal nanoparticles represent one of the advanced systems for the delivery of nucleic acids [18–23]. We developed a pH-sensitive MEND with a pH-sensitive lipid, YSK05 (YSK05-MEND), which has neutral surface at physiological pH, but develops a cationic surface in an acidic compartment such as endosomes/lysosomes [26,27]. In the present study, we attempted to utilize YSK05-MEND to deliver an anti-miR modified with 2′-OMe and PS linkage (AMO) to liver.

We first compared the YSK05-MEND with a commercially available reagent, LFN2k in murine hepatoma Hepa1c1c7 cells (Figs. 1 and 2). Despite its neutral surface charge, the AMO122-YSK05-MEND showed activity in the cultured cells (Fig. 1a). It was reported that neutral liposomes absorb apolipoprotein E (apoE) in the circulation, which enhances the uptake of the liposomes by hepatocytes *via* low-density lipoprotein (LDL) receptors (LDLRs) that are expressed on the surface of hepatocytes [30,31]. Since Hepa1c1c7 cells express LDLR (Fig. S3), it is likely that the YSK05-MEND was taken up by the cells *via* the interaction with LDLRs following the association of YSK05-MEND with apoE in the serum-containing culture media. On the other hand, a lipoplex composed of the cationic liposomal reagent LFN2k and AMO is taken up *via* endocytosis following its association with anionic molecules on the cell surface [32,33]. Despite the about 2 fold higher uptake of Cy5-AMO (Fig. 2b), the efficiency of AMO122 in LFN2k was inferior to that for the YSK05-MEND (Fig. 1a). It appears that the Cy5-AMOs delivered by LFN2k become trapped in endosomes/lysosomes or vesicular compartments because Cy5-AMOs become aggregated, as evidence by the appearance of a punctuate pattern (Fig. 2c). This suggests that LFN2k cannot escape efficiently from endosomal/lysosomal compartments. In contrast, the pattern for the signals for Cy5-AMO delivered by the YSK05-MEND was defused. With an apparent pKa of about 6.6 (Fig. S1b), the AMO122-YSK05-MEND becomes a cationic species in response to the acidic environment of early endosomes, which triggers membrane fusion with the endosomal membrane. Our previous study showed that the fusion activity of YSK05-MEND was dramatically superior to that of a MEND composed of a conventional cationic lipid, such as DOTAP [26]. This allows the AMOs encapsulated in the YSK05-MEND to efficiently escape from endosomes into the cytosol, which could result in the diffuse Cy5-AMO signals. For the reasons stated above, the pH-sensitive YSK05-MEND showed a higher activity than LFN2k. Furthermore, cytotoxicity was observed only in the LFN2k treated cells (Fig. 1b and c). Previous studies have reported that cationic lipids induce cytotoxicity including cell shrinking, thus reduced the level of mitosis and vacuolization of the cytoplasm [34]. Therefore, the neutral characteristics of the YSK05-MEND in the cytosol also contribute to the reduced cytotoxicity.

For *in vivo* evaluation, the YSK05-MEND encapsulating AMO122 was tested in comparison with free AMO122 because LFN2k cannot be

applied to systemic use, and chemically modified anti-miRs are largely used as the free form to regulate target miR-122 in liver [11]. Previous *in vivo* studies using mice reported that an effective miR-122 knockdown involves the use of a total intravenous dose of 240 mg/kg (80 mg/kg three times) of cholesterol-conjugated 2′-O-Me antagomir [3], total intraperitoneal doses of 100–600 mg/kg (12.5–75 mg/kg twice weekly for four weeks) of 2′-MOE oligonucleotides [4], a total intravenous dose of 75 mg/kg LNA-antimiR (25 mg/kg three consecutive days) [12], and a total intravenous dose of 60 mg/kg (20 mg/kg three times) of tiny LNA [14], which resulted in the lowering of a plasma cholesterol phenotype. These findings indicate that high doses are required to exert their function when anti-miRs are used as a free form, which can be attributed to the pharmacokinetic properties of anti-miRs. Small molecules having a molecular weight of <50 kDa or a diameter <6–8 nm are cleared from the systemic circulation by glomerular filtration in the kidney [16,17]. Since the molecular weight of anti-miRs is generally around 8 kDa, systemically administrated anti-miRs are largely eliminated *via* the kidney, which results the limited availability of anti-miR in hepatocytes and the need for high doses. It was reported that siRNA delivered by a stable nucleic acid lipid nanoparticle (SNALP) induced the knockdown of a target gene in the liver at lower doses (0.1–1 mg/kg) than that for a cholesterol conjugated siRNA (50–100 mg/kg) [19]. This suggests that drug delivery technologies could alter the pharmacokinetic properties of nucleic acids and permit their function to be exerted with a lower dose of nucleic acid. We evaluated whether YSK05-MEND was a valid route for the systemic delivery of AMO122 to the liver in comparison with the administration of free AMO122.

Prior to functional analysis, the distribution of Cy5-AMOs in the liver and kidney was evaluated. Systemically administrated free Cy5-AMO was found in the kidney and not in the liver (Fig. 3). In contrast, Cy5-AMO encapsulated in YSK05-MEND was mainly delivered to the liver with decreasing the accumulation of Cy5-AMO in the kidney compared to that for free Cy5-AMO because the diameter (about 70 nm) prevented the YSK05-MEND from being cleared by the renal route. As mentioned above, neutral liposomes acquire ApoE in the circulation, followed by hepatic uptake *via* LDLRs that are expressed on the surface of hepatocytes [30,31]. It was also reported that the average diameter of sinusoidal fenestrae in C57CL/B mice is 141 nm [35]. Being 70 nm in average diameter, the YSK05-MEND could pass through fenestrae and access hepatocytes. Therefore, it is reasonable to suppose that the YSK05-MEND was taken up by hepatocytes mediated by the association of ApoE with LDL receptors, which resulted in an enhanced delivery of AMOs to the livers in mice after systemic administration.

The three intravenous injections of AMO122-YSK05-MEND at a dose of 1 mg AMO/kg led to the efficient inhibition of miR-122 in the liver and an increase in *AldoA*, *Bckdk* and *Ndrg3* (Fig. 4a and b), while the treatment of free AMO122, the empty YSK05-MEND and the YSK05-MEND encapsulating AMO10b resulted in negligible change (Fig. S2). This suggests that the inhibition of miR-122 and subsequent increment in target genes can be attributed to the antagonism of miR-122 with AMO122. The inhibition persisted until at least day 12 (Fig. 5a, b and c). The durability of AMO122 delivered *via* the YSK05-MEND was consistent with a previous report [12]. It is well-known that chemical modification including 2′-O-Me and phosphorothioate linkages in oligonucleotides improve resistance to nucleases and the binding affinity to the target sequence compared to unmodified ones, which enhances and prolongs their effect [3,11,36,37]. It was suggested that chemically modified AMO122 remained intact for approximately 2 weeks in hepatocytes. However, in addition to the stability of AMO122, the half-lives of miR122, target genes, and cholesterol could also affect the time-dependent change, further study will be required to reveal the correct mechanism responsible for the inhibition of miR-122 by AMO122. In addition, the AMO122-YSK05-MEND caused no alterations in body weight or serum markers of liver toxicity, ALT (Fig. 5d and e), indicating that the YSK05-MEND is not associated with any serious acute toxicity.

5. Conclusion

In the present study, we demonstrated the delivery of AMO to hepatocytes by the intravenous administration of AMOs encapsulated in a pH-sensitive YSK05-MEND. The use of the AMO122-YSK05-MEND resulted in the efficient enhancement of *AldoA in vitro* owing to its ability to escape from endosomes in comparison with LFN2k. Systemically administrated Cy5-AMO formulated in YSK05-MEND was delivered to the liver rather than the kidney, whereas free Cy5-AMO mainly accumulated in the kidney due to its low molecular weight. Antagonism of the target miR-122 and the subsequent increase in the expression level of genes in the liver and the decrease in plasma cholesterol levels were induced by AMO122-YSK05-MEND at a total dose of 3 mg AMO/kg, while a comparable dose of free AMO122 had no effect. Even though anti-miRs are utilized in the free form for regulation of miRNA in clinical procedures, high doses are required. The present study demonstrates that the use of drug delivery technologies presents a practical and valuable alternative to anti-miRNA therapeutics. Collectively, YSK05-MEND represents a promising system for use in the *in vivo* delivery of AMO to the liver.

Acknowledgment

This work was supported in part by a Grant-in-Aid for Scientific Research on Innovative Area "Nanomedicine Molecular Science" (No. 2306), a Grant-in-Aid for Scientific Research (grant No. 23249008) from the Ministry of Education, Culture, Sports, Science and Technology (MEXT) in Japan and the Special Education and Research Expenses of MEXT. The authors also with to thank De. Milton S. Feather for his helpful advice in writing the English manuscript.

Appendix A. Supplementary data

Supplementary data to this article can be found online at http://dx.doi.org/10.1016/j.jconrel.2013.10.023.

References

[1] V. Ambros, The functions of animal microRNAs, Nature 431 (2004) 350–355.
[2] M. Lagos-Quintana, R. Rauhut, A. Yalcin, J. Meyer, W. Lendeckel, T. Tuschl, Identification of tissue-specific microRNAs from mouse, Curr. Biol. 12 (2002) 735–739.
[3] J. Krützfeldt, N. Rajewsky, R. Braich, K.G. Rajeev, T. Tuschl, M. Manoharan, M. Stoffel, Silencing of microRNAs *in vivo* with 'antagomirs', Nature 438 (2005) 685–689.
[4] Davis, S.F. Murray, X.X. Yu, S.K. Pandey, M. Pear, L. Watts, S.L. Booten, M. Graham, R. McKay, A. Subramaniam, S. Propp, B.A. Lollo, S. Freier, C.F. Bennett, S. Bhanot, B.P. Monia, miR-122 regulation of lipid metabolism revealed by *in vivo* antisense targeting, Cell Metab. 3 (2006) 87–98.
[5] C.L. Jopling, M. Yi, A.M. Lancaster, S.M. Lemon, P. Sarnow, Modulation of hepatitis C virus RNA abundance by a liver-specific microRNA, Science 309 (2005) 1577–1581.
[6] C. Coulouarn, V.M. Factor, J.B. Andersen, M.E. Durkin, S.S. Thorgeirsson, Loss of miR-122 expression in liver cancer correlates with suppression of the hepatic phenotype and gain of metastatic properties, Oncogene 28 (2009) 3526–3536.
[7] X. Tang, J. Gal, X. Zhuang, W. Wang, H. Zhu, G. Tang, A simple array platform for microRNA analysis and its application in mouse tissues, RNA 12 (2007) 1803–1822.
[8] A.P. Lewis, C.L. Jopling, Regulation and biological function of the liver-specific miR-122, Biochem. Soc. Trans. 38 (2010) 1553–1557.
[9] M.S. Ebert, J.R. Neilson, P.A. Sharp, MicroRNA sponges: competitive inhibitors of small RNAs in mammalian cells, Nat. Methods 4 (2007) 721–726.
[10] J. Xie, S.L. Ameres, R. Friedline, J.H. Hung, Y. Zhang, Q. Xie, L. Zhong, Q. Su, R. He, M. Li, H. Li, X. Mu, H. Zhang, J.A. Broderick, J.K. Kim, Z. Weng, T.R. Flotte, P.D. Zamore, G. Gao, Long-term, efficient inhibition of microRNRNA function in mice using rAAV vectors, Nat. Methods 9 (2012) 403–409.
[11] J. Stenvang, A. Petri, M. Lindow, S. Obad, S.J. Kauppinen, Inhibition of microRNA function by antimiR oligonucleotides, Silence 3 (2012) 1.
[12] J. Elmén, M. Lindow, A. Silahtaroglu, M. Bak, M. Christensen, A. Lind-Thomsen, M. Hedtjärn, J.B. Hansen, H.F. Hansen, E.M. Straarup, K. McCullagh, P. Kearney, S. Kauppinen, Antagonism of microRNA-122 in mice by systemically administered LNA-antimiR leads to up-regulation of a large set of predicted target mRNAs in the liver, Nucleic Acids Res. 36 (2008) 1153–1162.
[13] J. Elmén, M. Lindow, S. Schütz, M. Lawrence, A. Petri, S. Obad, M. Lindholm, M. Hedtjärn, H.F. Hansen, U. Berger, S. Gullans, P. Kearney, P. Sarnow, E.M. Straarup, S. Kauppinen, LNA-mediated microRNA silencing in non-human primates, Nature 452 (2008) 896–899.

[14] S. Obad, C.O. dos Santos, A. Petri, M. Heidenblad, O. Broom, C. Ruse, C. Fu, M. Lindow, J. Stenvang, E.M. Straarup, H.F. Hansen, T. Koch, D. Pappin, G.J. Hannon, S. Kauppinen, Silencing of microRNA families by seed-targeting tiny LNAs, Nat. Genet. 43 (2011) 37378.
[15] H.L. Janssen, H.W. Reesink, F.J. Lawitz, S. Zeuzem, M. Rodriguez-Torres, K. Patel, A.J. van der Meer, A.K. Patick, A. Chen, Y. Zhou, R. Persson, B.D. King, S. Kauppinen, A.A. Levin, M.R. Hodges, Treatment of HCV infection by targeting microRNA, N. Engl. J. Med. 368 (2013) 1685–1694.
[16] B. Haraldsson, J. Nyström, W.M. Deen, Properties of the glomerular barrier and mechanisms of proteinuria, Physiol. Rev. 88 (2008) 451–487.
[17] R.M. Bukowski, C. Tendler, D. Cutler, E. Rose, M.M. Laughlin, P. Statkevich, Treating cancer with PEG Intron: pharmacokinetic profile and dosing guidelines for an improved interferon-alpha-2b formulation, Cancer 95 (2002) 389–396.
[18] C.V. Pecot, G.A. Calin, R.L. Coleman, G. Lopez-Berestein, A.K. Sood, RNA interference in the clinic: challenges and future directions, Nat. Rev. Cancer 11 (2011) 59–67.
[19] T.S. Zimmermann, A.C. Lee, A. Akinc, B. Bramlage, D. Bumcrot, M.N. Fedoruk, et al., RNAi-mediated gene silencing in non-human primates, Nature 441 (2006) 111–114.
[20] S.C. Semple, A. Akinc, J. Chen, A.P. Sandhu, B.L. Mui, C.K. Cho, D.W. Sah, D. Stebbing, E.J. Crosley, E. Yaworski, I.M. Hafez, J.R. Dorkin, J. Qin, K. Lam, K.G. Rajeev, K.F. Wong, L.B. Jeffs, L. Nechev, M.L. Eisenhardt, M. Jayaraman, M. Kazem, M.A. Maier, M. Srinivasulu, M.J. Weinstein, Q. Chen, R. Alvarez, S.A. Barros, S. De, S.K. Klimuk, T. Borland, V. Kosovrasti, W.L. Cantley, Y.K. Tam, M. Manoharan, M.A. Ciufolini, M.A. Tracy, A. de Fougerolles, I. MacLachlan, P.R. Cullis, T.D. Madden, M.J. Hope, Rational design of cationic lipids for siRNA delivery, Nat. Biotechnol. 28 (2010) 172–176.
[21] M. Jayaraman, S.M. Ansell, B.L. Mui, Y.K. Tam, J. Chen, X. Du, D. Butler, L. Eltepu, S. Matsuda, J.K. Narayanannair, K.G. Rajeev, I.M. Hafez, A. Akinc, M.A. Maier, M.A. Tracy, P.R. Cullis, T.D. Madden, M. Manoharan, M.J. Hope, Maximizing the potency of siRNA lipid nanoparticles for hepatic gene silencing *in vivo*, Angew. Chem. Int. Ed. Engl. 51 (2012) 8529–8533.
[22] D. Yang, Y. Sun, L. Hu, H. Zheng, P. Ji, C.V. Pecot, Y. Zhao, S. Reynolds, H. Cheng, R. Rupaimoole, D. Cogdell, M. Nykter, R. Broaddus, C. Rodriguez-Aguayo, G. Lopez-Berestein, J. Liu, I. Shmulevich, A.K. Sood, K. Chen, W. Zhang, Integrated analyses identify a master microRNA regulatory network for the mesenchymal subtype in serous ovarian cancer, Cancer Cell 23 (2013) 186–199.
[23] S. Anand, B.K. Majeti, L.M. Acevedo, E.A. Murphy, R. Mukthavaram, L. Scheppke, M. Huang, D.J. Shields, J.N. Lindquist, P.E. Lapinski, P.D. King, S.M. Weis, D.A. Cheresh, MicroRNA-132-mediated loss of p120RasGAP activates the endothelium to facilitate pathological angiogenesis, Nat. Med. 16 (2010) 909–914.
[24] H. Hatakeyama, H. Akita, H. Harashima, A multifunctional envelope type nano device (MEND) for gene delivery to tumours based on the EPR effect: a strategy for overcoming the PEG dilemma, Adv. Drug Deliv. Rev. 63 (2011) 152–160(H. Hatakeyama, H. Akita, H. Harashima, Adv. Drug Deliv. Rev. (2011) 152–160).
[25] T. Nakamura, H. Akita, Y. Yamada, H. Hatakeyama, H. Harashima, A multifunctional envelope-type nanodevice for use in nanomedicine: concept and applications, Acc. Chem. Res. 45 (2012) 1113–1121.
[26] Y. Sato, H. Hatakeyama, Y. Sakurai, M. Hyodo, H. Akita, H. Harashima, A pH-sensitive cationic lipid facilitates the delivery of liposomal siRNA and gene silencing activity *in vitro* and *in vivo*, J. Control. Release 163 (2012) 267–276.
[27] Y. Sakurai, H. Hatakeyama, Y. Sato, M. Hyodo, H. Akita, H. Harashima, Gene silencing *via* RNAi and siRNA quantification in tumor tissue using MEND, a liposomal siRNA delivery system, Mol. Ther. 21 (2013) 1195–1203.
[28] S. Davis, B. Lollo, S. Freier, C. Esau, Improved targeting of miRNA with antisense oligonucleotides, Nucleic Acids Res. 34 (2006) 2294–2304.
[29] S.H. Hsu, B. Wang, J. Kota, J. Yu, S. Costinean, H. Kutay, L. Yu, S. Bai, K. La Perle, R.R. Chivukula, H. Mao, M. Wei, K.R. Clark, J.R. Mendell, M.A. Caligiuri, S.T. Jacob, J.T. Mendell, K. Ghoshal, Essential metabolic, anti-inflammatory, and anti-tumorigenic functions of miR-122 in liver, J. Clin. Invest. 122 (2012) 2871–2883.
[30] X. Yan, F. Kuipers, L.M. Havekes, R. Havinga, B. Dontje, K. Poelstra, G.L. Scherphof, J.A. Kamps, The role of apolipoprotein E in the elimination of liposomes from blood by hepatocytes in the mouse, Biochem. Biophys. Res. Commun. 328 (2005) 57–62.
[31] A. Akinc, W. Querbes, S. De, J. Qin, M. Frank-Kamenetsky, K.N. Jayaprakash, M. Jayaraman, K.G. Rajeev, W.L. Cantley, J.R. Dorkin, J.S. Butler, L. Qin, T. Racie, A. Sprague, E. Fava, A. Zeigerer, M.J. Hope, M. Zerial, D.W. Sah, K. Fitzgerald, M.A. Tracy, M. Manoharan, V. Koteliansky, A.D. Fougerolles, M.A. Maier, Targeted delivery of RNAi therapeutics with endogenous and exogenous ligand-based mechanisms, Mol. Ther. 18 (2010) 1357–1364.
[32] K.A. Mislick, J.D. Baldeschwieler, Evidence for the role of proteoglycans in cation-mediated gene transfer, Proc. Natl. Acad. Sci. U.S.A. 93 (1996) 12349–12354.
[33] L.C. Mounkes, W. Zhong, G. Cipres-Palacin, T.D. Heath, R.J. Debs, Proteoglycans mediate cationic liposome-DNA complex-based gene delivery *in vitro* and *in vivo*, J. Biol. Chem. 273 (1998) 26164–26170.
[34] H. Lv, S. Zhang, B. Wang, S. Cui, J. Yan, Toxicity of cationic lipids and cationic polymers in gene deliver, J. Control. Release 114 (2006) 100–109.
[35] J. Snoeys, J. Lievens, E. Wisse, F. Jacobs, H. Duimel, D. Collen, P. Frederik, B.D. Geest, Species differences in transgene DNA uptake in hepatocytes after adenoviral transfer correlate with the size of endothelial fenestrae, Gene Ther. 14 (2007) 604–612.
[36] J. Krützfeldt, S. Kuwajima, R. Braich, K.G. Rajeev, J. Pena, T. Tuschl, M. Manoharan, M. Stoffel, Specificity, duplex degradation and subcellular localization of antagomir, Nucleic Acids Res. 35 (2007) 2885–2892.
[37] M. Takahashi, C. Nagai, H. Hatakeyama, N. Minakawa, H. Harashima, A. Matsuda, Intracellular stability of 2′-OMe-4′-thioribonucleoside modified siRNA leads to long-term RNAi effect, Nucleic Acids Res. 40 (2012) 5787–5793.

International Journal of Pharmaceutics 456 (2013) 195–201

Contents lists available at ScienceDirect

International Journal of Pharmaceutics

journal homepage: www.elsevier.com/locate/ijpharm

Pharmaceutical nanotechnology

A liposomal delivery system that targets liver endothelial cells based on a new peptide motif present in the ApoB-100 sequence

Afsana Akhter[a,c], Yasuhiro Hayashi[a,c], Yu Sakurai[a,c], Noritaka Ohga[b,c], Kyoko Hida[b,c], Hideyoshi Harashima[a,b,c,*]

[a] Laboratory of Innovative Nanomedicine, Faculty of Pharmaceutical Sciences, Hokkaido University, Kita 12, Nishi 6, Kita-ku, Sapporo 060-0812, Japan
[b] Laboratory for Molecular Design of Pharmaceutics, Faculty of Pharmaceutical Sciences, Hokkaido University, Kita-12, Nishi-6, Kita-ku, Sapporo, Hokkaido 060-0812, Japan
[c] Division of Vascular Biology, Graduate School of Dental Medicine, Hokkaido University, Kita 13 Nishi 7, Kita-ku, Sapporo 060-0812, Japan

ARTICLE INFO

Article history:
Available online 7 August 2013

Keywords:
ApoB-100 sequence
CSPG
LDL receptor
Liver endothelial cell
RLTR peptide
KLGR peptide

ABSTRACT

Liver dysfunction is associated with a variety of liver diseases, including viral or alcoholic hepatitis, fibrosis, cirrhosis, and portal hypertension. A targeted drug delivery system would be very useful in the treatment of these diseases. We herein describe the development of a system comprised of a new peptide–lipid conjugate for the efficient delivery of molecules to LEC. The RLTRKRGLK sequence (3359–3367), which mediates the association of LDL with arterial CSPG and an LDL receptor, was utilized as a ligand for achieving this goal. The peptide modified PEG-LPs (RLTR-PEG-LPs) were efficiently taken up by primary liver endothelial cells (liver ECs) and other types of cells. In vivo biodistribution and confocal microscopy analysis showed that RLTR-PEG-LPs became widely accumulated in LECs within a short time. Distribution of RLTR-PEG-LPs was greatly reduced with a pretreatment of unlabeled RLTR-PEG-LPs, not cationic LPs, indicating that the sequence is important for LECs. The findings indicate that a reverse sequence of RLTR (KLGR) modified PEG-LPs (KLGR-PEG-LP) did the same pattern compared with RLTR-PEG-LPs, suggesting that the RKR or RXXR sequence might be essential for LECs targeting. Collectively RLTR-PEG-LPs and KLGR-PEG-LPs have the potential for delivering drugs to LECs.

1. Introduction

The liver is the largest organ of the body and is probably the most important power and sewage treatment plant in the body. Two major types of cells populate the liver, namely, parenchymal and non-parenchymal cells. Approximately 80% of the liver volume is made up of parenchymal cells commonly referred to as hepatocytes (Ramadori et al., 2008). Sinusoidal endothelial cells, Kupffer cells and hepatic stellate cells are examples of non-parenchymal cells. Different types of liver diseases are associated with different types of liver cells. For example viral hepatitis and alcoholic hepatitis are associated with hepatocytes. Liver endothelial cell (LEC) dysfunction is associated with variety of liver diseases, including fibrosis, cirrhosis, and portal hypertension (Dominique and Vijay, 2010). The defenestration of liver endothelial cells causes hyperlipidemia, because it becomes difficult for lipoproteins to reach hepatocytes (Rajkumar et al., 2010). Kupffer cells are associated with the progression of non-alcoholic steatosis and fibrosis. It has also been reported that hepatocellular stress caused by various diseases causes the release of different types of cytokines and chemokines by different types of cells which ultimately cause the transmigration of inflammatory cells toward their target, hepatocytes (Ramadori et al., 2008). Therefore, a selective drug delivery system would be an ideal approach for achieving a subsequent efficient therapy for treating different types of liver diseases.

A group of certain basic proteins or peptides have the ability to inhibit the binding of low density lipoprotein (LDL) to its receptor protein (Brown et al., 1978). This inhibition is caused by polycations interacting with the receptor. LDLs are associated with a negatively charged LDL receptor even though the net charge of this lipoprotein is also negative. This suggests that the net charge of the LDL is governed by the positive charge of the ApoB sequence. Two basic regions of similar size in ApoB-100 segments, namely 3147 through 3157 and 3359 through 3367 are part of the LDL receptor binding domain. This ApoB heterodimer binds to the LDL receptor and also binds with Glycoseaminoglycans (GAGs) with an affinity similar to that between LDL and GAGs (Urban et al., 1997). The ApoB-100 segment RLTRKRGLK (3359–3367) is a mediator of the association between LDL and arterial Chondroitin sulfate-rich proteoglycan

* Corresponding author at: Faculty of Pharmaceutical Sciences, Hokkaido University, Kita-12, Nishi-6, Kita-ku, Sapporo, Hokkaido 060-0812, Japan.
Tel.: +81 11 706 3919; fax: +81 11 706 4879.
E-mail address: harasima@pharm.hokudai.ac.jp (H. Harashima).

0378-5173/$ – see front matter © 2013 Elsevier B.V. All rights reserved.
http://dx.doi.org/10.1016/j.ijpharm.2013.07.068

(CSPG) (Urban et al., 1993). It has recently been reported that LEC express low density lipoprotein receptor protein-1 (LRP-1) which is a member of the LDL receptor gene family (Oie et al., 2011; Thomas et al., 1999). Another study has shown that LDL is taken up by both parenchymal and non-parenchymal cells (Marit et al., 1998).

Liposomes are suitable nano-carriers that have the capacity to deliver drug particles to various target cells in vitro or diseased tissues in vivo (Puri et al., 2009; Du et al., 2007). Based on these considerations, we selected the ApoB segment RLTRKRGLK (3359–3367) abbreviated here as RLTR for use as a novel ligand in designing a selective targeting system for hepatocytes. Surprisingly, however, this carrier system was accumulated through the blood vessels in the liver. In order to examine the targeting ability of this RLTR modified liposome, our efforts were focused on two parameters, one being the cationic nature of this peptide and second the essential peptide sequence.

2. Materials and methods

2.1. Materials

Cholesterol (Chol), 1,2-dioleoyl-sn-glycero-3-phosphoethanolamine (DOPE), diethanolamine chloride (DC-6-14), Egg phosphatidylcholine (EPC), N-(lissamine rhodamine B sulfonyl) -1,2-dioleoyl-sn-glycero-3-phosphoethanolamine (rhodamine -DOPE), 1,2-distearoyl-*sn*-glycero-3-phosphoethanolamine-N-[methoxy (polyethyleneglycol)-2000] (PEG_{2000}-DSPE) were purchased from Avanti Polar Lipids (Alabaster, AL, USA). N-[(3-maleimide-1-oxopropyl) aminopropyl polyethyleneglycol-carbamyl] distearoylphosphatidyl-ethanolamine (maleimide-PEG-DSPE) was purchased from Nippon Oil and Fat Co. (Tokyo, Japan). ^{3}H-Cholesteryl hexadecyl ether (CHE) were purchased from New England Nuclear (USA). RLTRKRGLKGGC (RLTR in brief) and KLGRKRTLRGGC (KLGR in brief) peptides were purchased from Kurabo Industries, Osaka, Japan. Endothelial Cell Basal Medium (EBM-2) and other related growth factors were purchased from Lonza (Walkersville, MD, USA). Dulbecco's fetal bovine serum (FBS) was obtained from Hyclone Laboratories (Logan, UT, USA). All other chemicals used in this study were of analytical grade.

2.2. Animals

4–5 week old male ICR mice were purchased from Japan SLC (Shizuoka, Japan). The experimental protocols were reviewed and approved by the Hokkaido University Animal Care Committee in accordance with the guidelines for care and use of Laboratory animals. Animals were used without fasting in all experiments.

2.3. Conjugation of the RLTR peptide to PEG_{2000}-DSPE

Peptides conjugated with glycine–glycine–cysteine (GGC) sequence at the N-terminal were purchased from commercial sources. Actually the GGC linker was added to the N-terminal to facilitate the binding of the thiol group of cysteine residue to the pyrrole group of Maleimide-PEG_{2000}-DSPE. The additional Gly-Gly (GG) amino acid was added to increase the flexibility of the peptide ligand attached on the top of Mal-PEG_{2000}-DSPE. Conjugation was achieved by incubating a 1.2:1 molar ratio of RLTRKRGLKGGC peptide and maleimide-PEG-DSPE in deionized water at room temperature for 24 h. The conjugation of RLTR with PEG was confirmed by matrix assisted laser desorption/ionization-time of flight (MALDI-TOF) MS (Bruker Daltonics, Germany) using acetonitrile:water = 7:3 with 0.1% of trifluoroacetate as the matrix solution, supplied with a 10 mg/ml solution of dihydroxybenzoic acid.

2.4. Preparation of liposomes

Liposomes (LPs) composed of EPC/Chol (molar ratio: 7/3) was prepared by the lipid hydration method. A control cationic LP was prepared using DC6-14, DOPE, and Cholesterol at a molar ratio of 4:3:3 (Ishiwata et al., 2000). RLTR peptide modified PEG-LPs (RLTR-PEG-LPs) were prepared by adding the required amount of RLTR-PEG to the lipid solution. 1 mol% rhodamine-DOPE was incorporated, to serve as a label for the lipid component. A lipid film was produced by evaporation of the solvents (chloroform and ethanol) from a lipid solution in a glass tube. HEPES buffer (10 mM, pH 7.4) was added and the solution was incubated for 10 min to hydrate the lipid film. The glass tube was then sonicated for approximately 30 s in a bath-type sonicator (AU-25C, Aiwa, Tokyo, Japan). The mean size and zeta potential of the prepared LPs were determined using a Zetasizer Nano ZS ZEN3600 instrument (Malvern Instruments Ltd., Worchestershire, UK).

2.5. Isolation of primary liver endothelial cells (liver ECs)

Liver endothelial cells (liver ECs) were isolated as previously described (Hida et al., 2004; Akino et al., 2009; Ohga et al., 2009). Briefly, the liver of a female KSN mouse was excised. The excised tissue was minced and digested with collagenase II (Worthington, Freehold, NJ). Blood cells were removed by a single sucrose step-gradient centrifugation with Histopaque 1077 (Sigma-Aldrich), and the resulting cell suspension was filtered. Endothelial cells were isolated using MACS according to the manufacturer's instructions using a FITC-anti-CD31 antibody. CD31-positive cells were sorted and plated on 1.5% gelatin-coated culture plates and grown in EGM-2MV (Clonetics, Walkersville, MD) and 10% fetal bovine serum. After subculturing for 2 weeks, the isolated ECs were purified by a second round of purification using FITC-BS1-B4 (Vector Laboratories, Burlingame, CA). All of the endothelial cells were split at a ratio of 1:3.

2.6. In vitro cellular uptake study

For the cellular uptake study, 40,000 cells were seeded in a 24-well plate (Corning incorporated, Corning, NY, USA) (40,000 cells/well). After 24 h, the prepared rhodamine labeled PEG-LPs/RLTR-PEG-LPs were added and incubated for an additional 3 h. After the incubation, the cells were washed with PBS (pH 7.4) and then treated with Reporter Lysis Buffer (Promega Corp., Madison, WI, USA) followed by centrifugation at 12,000 rpm for 5 min at 4 °C to remove debris. The supernatants were then collected. The cellular uptake efficiency of the prepared rhodamine labeled LPs were determined by measuring the fluorescence intensity of rhodamine (excitation at 550 nm and emission at 590 nm) using FP-750 Spectrofluorometer (JAS Co., Tokyo, Japan).

2.7. In vivo biodistribution study

^{3}H-Cholesteryl hexadecyl ether (CHE) labeled LPs and RLTR-PEG-LPs were used to measure the biodistribution of liposomes in different organs in the mice. ICR mice were intravenously injected with ^{3}H-labeled LPs or RLTR-PEG-LPs. After 25 min, the animals were sacrificed; the portal vein was cut and a needle was introduced into the vena cava and 10–15 ml of heparin containing PBS (40 units/ml) solution was used to remove the remaining blood and cell surface bound RLTR-PEG-LPs in the liver. Other organs, including the lungs and kidney were also collected and all of the collected organs were weighed. After weighing, the samples were solubilized in Soluene-350 (Perkin-Elmer Life Sciences, Japan) for overnight at 55 °C. Samples were decolorized by treatment with H_2O_2. The radioactivity of the samples was

measured by using a liquid scintillation counting (LSC-6100, Aloka, Japan) after adding 10 ml of Hionic Flour (Perkin-Elmer Life Sciences, Japan) (Hatakeyama et al., 2004). Tissue accumulation of LPs was represented as the percentage of injected dose (%ID) per organ.

2.8. Confocal microscopy experiment

ICR mice were given intravenous injection of rhodamine labeled RLTR-PEG-LPs and the mice were killed 25 min after the treatment. The liver was perfused as mentioned in Section 2.7 and then it was collected. The liver was then excised and washed with saline and sliced into 10–15 mm-sized blocks with scissors. The liver sections were then incubated with a 20 fold volume of a diluted solution of Hoechst 33342 (1 mg/ml) and Isolectin B4 in HEPES buffer for 1 h. The specimens were placed on a 35 mm glass base dish (IWAKI, Osaka, Japan) and observed by confocal laser scanning microscopy (A1 Confocal Laser Microscope System, Nikon Instruments Inc., Tokyo, Japan).

2.9. Inhibition assay

2.9.1. In vivo competitive inhibition study of RLTR-PEG-LPs

ICR mice were injected with unlabeled LPs and after 15 min, they were injected with cationic LP or RLTR modified PEG-LP or KLGR (reverse peptide sequence of RLTR) modified PEG-LP. After another 25 min of incubation the mice were sacrificed and the livers were perfused with 10 ml of a 40% heparin-PBS solution. The mice livers were then collected, sliced into 0.5 mm × 0.5 mm pieces, stained with Hoechst 33342 and Isolectin B4 and then observed by confocal microscopy (A1 Confocal Laser Microscope System, Nikon Instruments Inc., Tokyo, Japan).

2.9.2. In vitro competitive inhibition study of RLTR-PEG-LPs

For in vitro inhibition study unlabeled RLTR-PEG or KLGR-PEG modified LPs were used as inhibitors. We previously used an excess amount of free RLTR or KLGR peptide as an inhibitor but no significant inhibition was observed (data not shown). It was reported that the monomeric free peptide might not be sufficiently effective to inhibit the interactions of multiplex RLTR-PEG-LP or KLGR-PEG-LP with the target receptor (Kibria et al., 2011). As a result we used unlabeled RLTR-PEG or KLGR-PEG modified LP as inhibitors in order to achieve multivalent attachment with the targeted receptors. Here 40,000 LECs were seeded in a 24-well plate and the plate was incubated overnight. After 24 h, different concentrations of rhodamine labeled and unlabeled PEG-LPs (1:0, 1:5, 1:10, 1:20 and 1:50 respectively) were added and incubated for 3 h. After 3 h, the cells were washed 3 times with 1 ml of ice-cold phosphate buffer saline (PBS) which was supplemented with heparin (20 units/ml) to completely remove the surface-bound RLTR-PEG-LP and the intracellular fluorescence intensity of rhodamine was then determined (Kibria et al., 2011).

Table 1
Physicochemical properties of the RLTR-PEG-LP.

% PEG	Properties			
	PEG-LP		RLTR-PEG-LP	
	Size (nm)	Z-potential (mV)	Size (nm)	Z-potential (mV)
0	92 ± 10	−5 ± 9	–	–
1	102 ± 8	−8 ± 5	115 ± 10	12 ± 4
3	100 ± 5	−20 ± 8	121 ± 14	20 ± 6
5	105 ± 7	−19 ± 11	135 ± 8	22 ± 8
10	110 ± 11	−24 ± 12	132 ± 10	27 ± 3

Data are presented as the mean ± SD ($n = 3$).

2.10. Statistical analysis

Comparisons between multiple treatments were made using one-way analysis of variance (ANOVA), followed by the 'Dunnett test'. Pair-wise comparisons of subgroups were made using the student's *t*-test. Differences among the means were considered to be statistically significant at a *P*-value of <0.05 and <0.01.

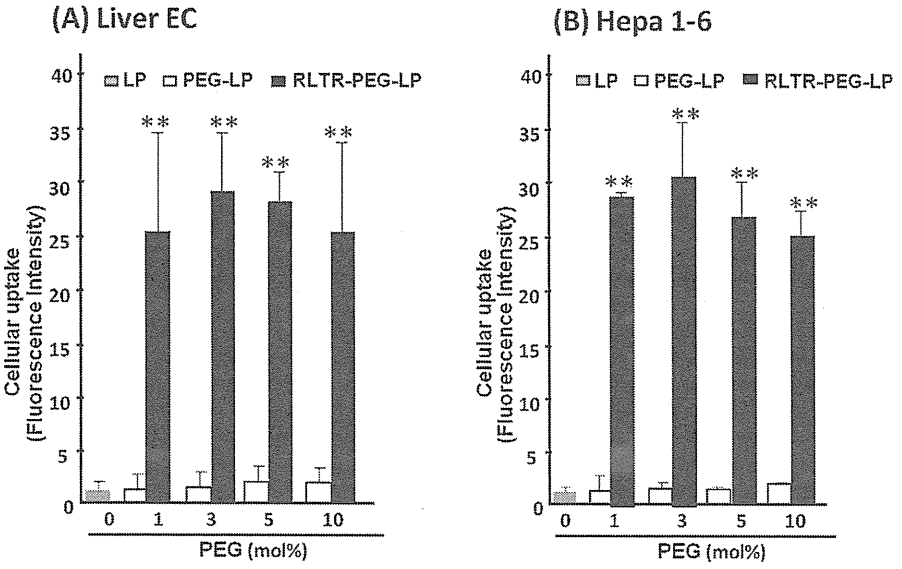

Fig. 1. Cellular uptake of RLTR-PEG-LPs. For the cellular uptake study, 40,000 cells/well were seeded in a 24-well plate. After 24 h LPs modified with different mol% of PEG-DSPE or RLTR-PEG-DSPE were incubated with (A) liver EC or (B) Hepa1-6 cells for 3 h and the cellular uptake efficiency of the prepared rhodamine labeled LPs were determined by measuring the fluorescence intensity of rhodamine. Cellular uptake is expressed as the mean ± SD ($n = 3$) and statistical analysis vs. LP was performed by One-way ANOVA followed by Dunnett-test. $^{**}P < 0.01$.

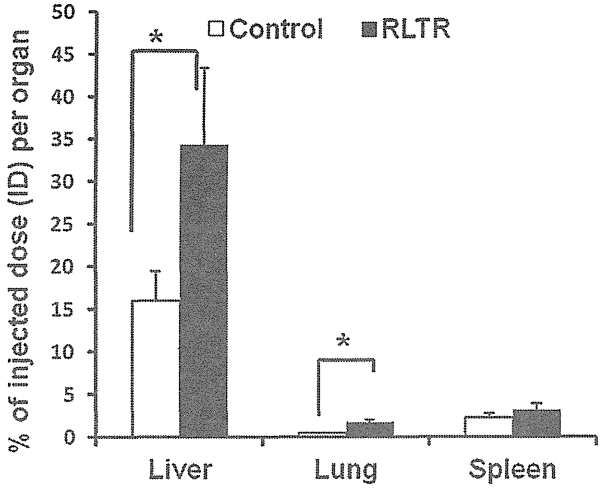

Fig. 2. Biodistribution of ^{3}H-CHE labeled RLTR-PEG-LPs and LPs in different organ. Male ICR mice were intravenously injected with labeled RLTR-PEG-LPs and LPs. After 25 min of incubation different organs of mouse were collected and radioactivity was measured. Tissue accumulation of LPs was represented as % of injected dose (ID). Here, % of ID is expressed as the mean ± SD ($n = 4$). Statistical analyses were performed by the unpaired Student's t-test, where $^{*}P < 0.05$.

3. Results

3.1. Synthesis of RLTR-PEG-DSPE

The thiol group of the cystein residue in the RLTR peptide was conjugated by reaction with Mal-PEG$_{2000}$-DSPE at 37 °C for 24 h (Reaction scheme is shown in the supplementary figure 1). MALDI-TOF MS analyses confirmed the synthesis of RLTR-PEG-DSPE.

Supplementary material related to this article can be found, in the online version, at http://dx.doi.org/10.1016/j.ijpharm.2013.07.068.

3.2. The characteristic of RLTR-PEG-LPs and its cellular uptake

The selected RLTR peptide was attached to the top of PEG in PEGylated liposomes. PEG liposomes (PEG-LPs) and RLTR modified PEG liposomes (RLTR-PEG-LPs) were prepared by incorporating PEG-DSPE or RLTR-PEG-DSPE at levels of 1, 3, 5, or 10 mol% of the total lipid. The physical properties of the prepared LPs are shown in Table 1. To evaluate the effect of the RLTR peptide on cellular uptake, we next examined the cellular uptake of RLTR-PEG-LPs and PEG-LPs in primary liver endothelial cells (LECs) and in Hepa1-6 cell line. The RLTR peptide enhanced the cellular uptake of PEG-LPs and the maximum cellular uptake was observed within 3 mol% of RLTR peptide modification in both the cells (Fig. 1A and B).

3.3. In vivo selectivity of RLTR peptide

A biodistribution study of RLTR-PEG-LPs was carried out in order to confirm the targeting ability of RLTR-PEG modified LP. Compared to unmodified control LPs, RLTR-PEG-LPs were largely accumulated in the liver, with only negligible accumulation in the lung or spleen, within a very short time (Fig. 2). The liver targeting ability of RLTR peptide was more than its ability to target lung or spleen. We then obtained an in vivo image of the liver to check the distribution pattern of this RLTR-PEG modified LP in liver.

We then performed an in vivo accumulation study to verify our hypothesis outlined in the introduction part. We investigated the intrahepatic distribution of RLTR-PEG-LPs by confocal microscopy. Rhodamine-labeled RLTR-PEG-LPs were widely distributed throughout the blood vessels (Fig. 3A), and these intensities were essentially merged with the signal for Isolectin B4, a marker of endothelial cells (Fig. 3B and C). These results demonstrate that RLTR-PEG-LPs efficiently target liver endothelial cells rather than hepatocytes. Furthermore, we compared the intrahepatic distribution pattern with RLTR-PEG-LPs and cationic LPs in order to evaluate the effect of the cationic charge of the liposomal surface. The size and zeta-potential of the rhodamine-labeled RLTR-PEG-LPs and cationic LPs was 125 nm, 26 mV and 132 nm, 22 mV respectively. The intrahepatic distribution pattern of the cationic

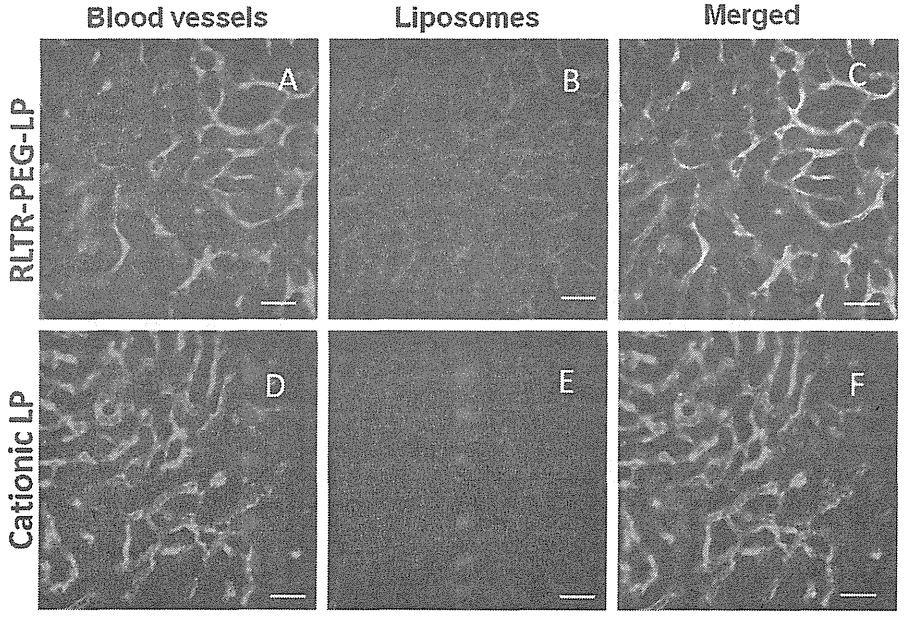

Fig. 3. Representative intrahepatic distribution pattern of RLTR-PEG-LPs (A–C) and a cationic control LPs, in which the lipid composition was DC6-14/DOPE/Chol = 4:3:3 (D–F). Green and red color represents blood vessels stained by Isolectin B4 and rhodamine labeled LPs respectively. Scale bars correspond to 50 μm in all images.

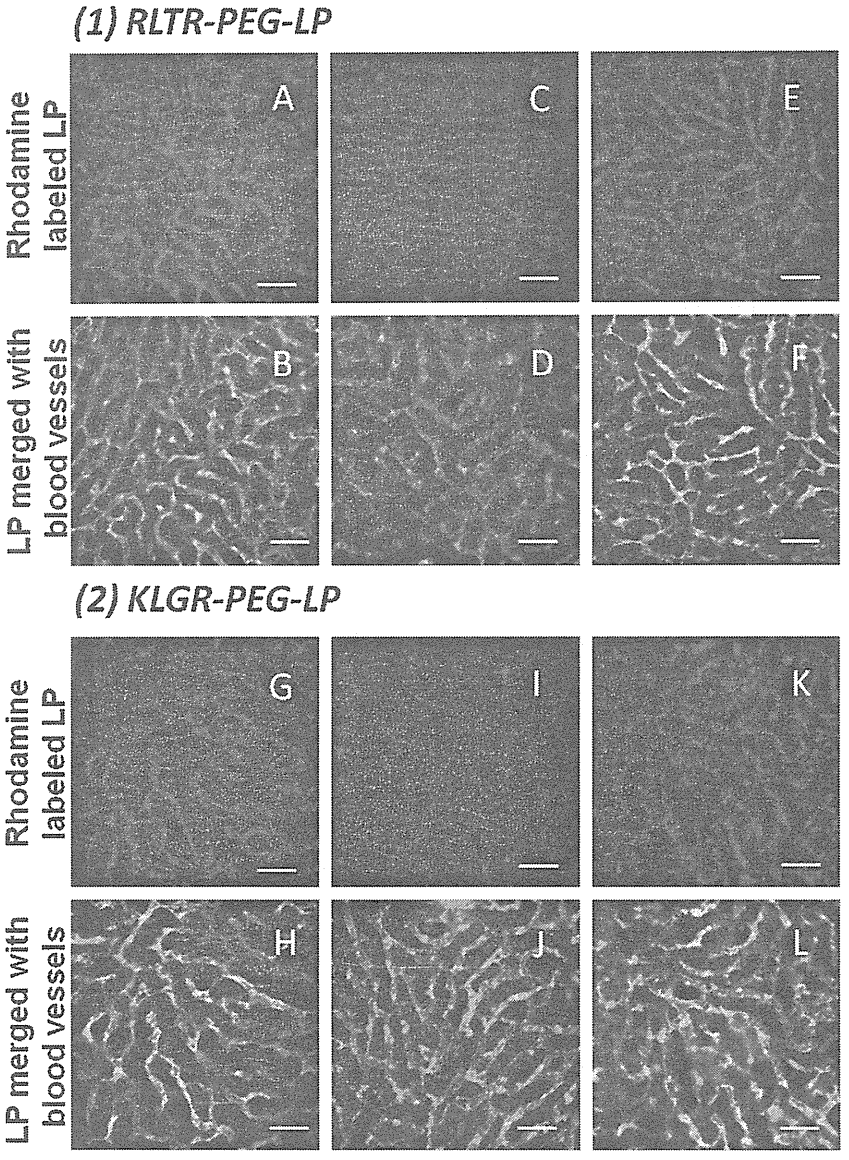

Fig. 4. In vivo competitive inhibition studies of RLTR-PEG-LPs or KLGR-PEG-LPs using unlabeled RLTR-PEG-LPs or KLGR-PEG-LPs or cationic LPs. Green and red color represents blood vessels stained by Isolectin B4 and rhodamine labeled LPs respectively. Mice were pretreated with unlabeled RLTR-PEG-LPs or KLGR-PEG-LPs or cationic LPs 15 min before the second treatment with labeled RLTR-PEG-LPs or KLGR-PEG-LPs for another 25 min of incubation. Representative images of liver tissues with (A and B) labeled RLTR-PEG-LPs, (C and D) labeled RLTR-PEG-LPs pre-treated with unlabeled RLTR-PEG-LPs, (E and F) labeled RLTR-PEG-LPs pre-treated with unlabeled cationic LPs, (G and H) labeled KLGR-PEG-LPs, (I and J) labeled KLGR-PEG-LPs pre-treated with unlabeled KLGR-PEG-LPs, (K and L) labeled KLGR-PEG-LPs pre-treated with unlabeled cationic LPs are shown. Scale bars correspond to 50 μm in all images.

LPs was quite different from that of the RLTR-PEG-LPs, in which the cationic LPs were gathered in particular spots (Fig. 3D). In addition, these dots did not overlap with liver endothelial cells (Fig. 3E and F) indicating that they were taken up by non-parenchymal cells such as Kupffer cells or were merely aggregated LPs.

3.4. In vivo inhibition study

In order to examine some possible mechanisms of unique targeting ability of RLTR peptide into liver endothelial cells, comparative studies of RLTR and its reversed peptide sequence named as KLGR were performed in the following part. Both RLTR-PEG-LPs and KLGR-PEG-LPs were accumulated along with the liver blood vessels (Fig. 4A and B, G and H). Next, accumulation of both labeled RLTR-PEG-LPs and KLGR-PEG-LP along with the liver blood vessels were dramatically inhibited by a pre-treatment with unlabeled RLTR-PEG-LPs or KLGR-PEG-LPs (Fig. 4C and D, I and J), however, small portions of signal were remaining. In contrast, the accumulation of both labeled RLTR-PEG-LPs or KLGR-PEG-LP was not reduced by the pre-treatment with unlabeled cationic LPs (Fig. 4E and F, K and L). The results generated in this study suggest that cationic charge is not the reason for this uptake and may be both RLTR peptide and its reverse sequence, the KLGR peptide has some specificity for liver endothelial cells. Possible interpretations will be discussed in Section 4.

3.5. In vitro comparative inhibition study of RLTR-PEG-LPs

This experiment was performed to support the in vivo inhibition data. We compared the cellular uptake of both RLTR-PEG-LPs and

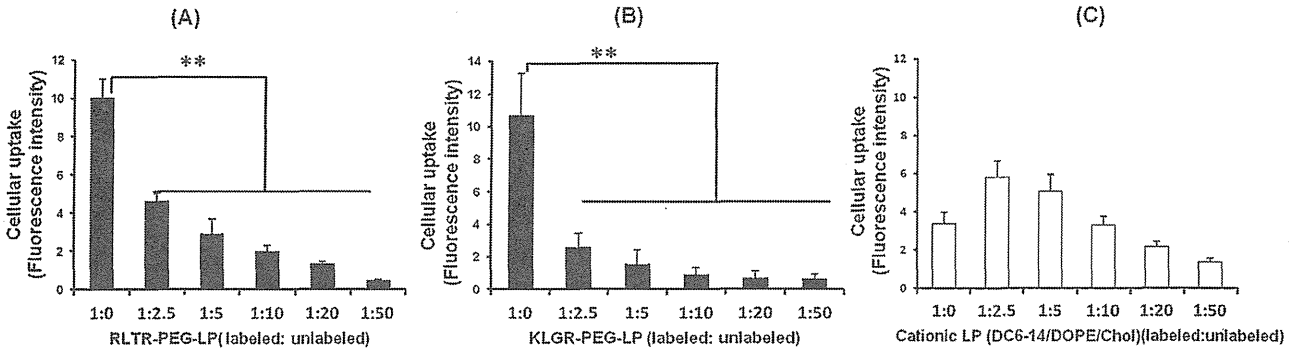

Fig. 5. In vitro cellular uptake inhibition studies using unlabeled (A) RLTR-PEG-LPs, (B) KLGR-PEG-LP and (C) cationic LPs. Different ratios of labeled and unlabled LPs were co-incubated with 40,000 liver ECs for 3 h. Data were expressed as the mean ± SD ($n = 3$). Statistical differences vs. RLTR-PEG-LP (1:0) or KLGR-PEG-LP (1:0) or control LP (1:0) were determined by one-way ANOVA followed by Dunnett test. $^{**}P < 0.01$.

KLGR-PEG-LPs with that of cationic-LPs under the inhibition with unlabeled RLTR-PEG-LPs or cationic-LPs. A comparative inhibition study with labeled and unlabeled LPs showed that the cellular uptake of labeled RLTR-PEG-LPs and KLGR-PEG-LPs were inhibited remarkably in the presence of a low amount of unlabeled RLTR-PEG-LPs and KLGR-PEG-LPs respectively (Fig. 5A and B). On the other hand, the cellular uptake of labeled cationic LPs was not inhibited to a significant extent by unlabeled cationic LPs (Fig. 5C). The results generated in this study suggest that both the RLTR and KLGR peptide efficiently delivered the nanocarriers into cells via a specific route, while cationic LPs were randomly taken up by cells. This conclusion is further supported by the in vivo comparative inhibition study.

4. Discussion

It has been reported that hepatocytes also express LDL receptors (Marit et al., 1998) and hepatocytes comprise 80% of the total liver volume (Kmieć, 2001). In a recent study it was also demonstrated that LDL is taken up by liver endothelial cells (Marit et al., 1998). In this present study we attempted to design a new ligand for hepatocytes based on the ApoB-100 sequence of LDL. The newly designed peptide ligand is referred to as RLTR. The size of the RLTR-PEG-LPs increased with the increase of the amount of RLTR-PEG. The surface charge of the PEG-LPs remained negative. However, the addition of the RLTR peptide resulted in a gradual increase in the surface charge of the PEG-LPs and a large difference in surface charge was observed between increments of RLTR-PEG of 1–10 mol% (Table 1). This increment in surface charge of the RLTR-PEG-LPs reflects the cationic properties of the RLTR peptide. RLTR-PEG-LPs showed a remarkable enhancement in cellular uptake compared to PEG-LPs in different cell types including liver endothelial cell and Hepa1-6 cell lines (Fig. 1). In the biodistribution study it was also observed that most of the RLTR modified PEG-LP had accumulated in the liver rather than other organs such as lung or spleen (Fig. 2). However, in confocal microscopy images it was observed that, RLTR-PEG-LPs accumulated at high levels in liver blood vessels (Fig. 3A–C) which indicate that these liposomes do not accumulate in hepatocytes. The cellular accumulation of RLTR-PEG-LPs was significantly higher than that of cationic LPs (Fig. 3D–F). Though the RLTR peptide is designed from LDL and there is previous report that LDL is rapidly taken up by LDL recep-

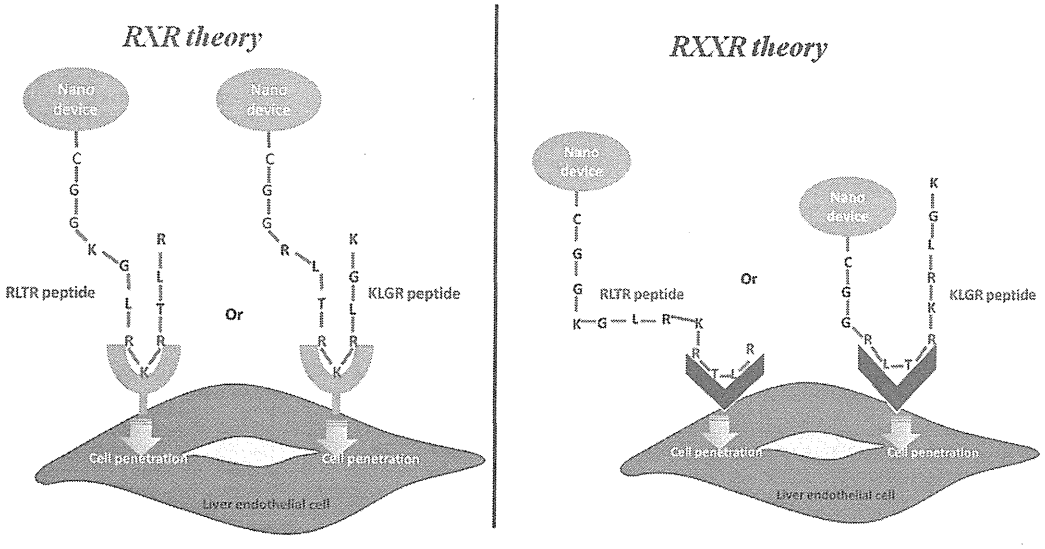

Fig. 6. Proposed theory for similar binding and cell penetration of RLTR and KLGR (reverse sequence of RLTR peptide) modified PEG-LPs. Where (A) shows binding of the RXR motif in both the peptide modified LPs with the receptor expressed by LEC and (B) shows binding of RXXR (RXXR represents either RLTR or RTLR motif) of RLTR or KLGR modified LPs respectively to the receptor expressed by LEC.

tors, the peptide modified PEG-LP is highly accumulated in liver EC. It is possible that this carrier system has more specificity for liver EC, rather than hepatocytes. This surprising accumulation of this carrier system through blood vessels led us to conclude that this nanoparticle might be an ideal system for targeting the liver endothelial cells. The finding that cationic peptides and lipids accumulate at high levels in endothelial cells of liver is attractive and interesting. There are very few reports of the use of cationic or neutral nano carriers to target liver endothelial cells (Bartsch et al., 2004; Toriyabe et al., 2011). It should be noted that, these systems failed to achieve high accumulation in liver endothelial cells. Because of this, in this study we seized the opportunity to develop this nanocarrier to target liver EC. There are two possible reasons for the high accumulation of RLTR modified PEG-LP in liver EC. Either the high cationic charge of the peptide is causing this high accumulation or the peptide sequence itself has specificity for liver endothelial cell. We then checked the specificity of both RLTR and its reverse sequence KLGR modified PEG-LP by both an in vitro and in vivo inhibition study. In the in vivo inhibition study we demonstrated that both the RLTR-PEG-LPs and KLGR-PEG-LPs uptake were inhibited by unlabeled RLTR-PEG-LPs and KLGR-PEG-LPs respectively (Fig. 4). However, the cationic LPs did not affect its uptake both in vivo or in vitro (Figs. 4 and 5). Given these findings, the possibility of a higher accumulation in LEC is due to a higher cationic charge can be excluded. We then attempted to address the second possible reason of the higher accumulation in LEC, namely, the sequence of the peptide. We found that the sequence contain a motif RKR which remains the same both in the RLTR and KLGR peptide, although the sequence is completely reversed. It has been reported that stearylated polyarginine and its derivatives, i.e. stearyl-$(RXR)_4$ mediates the efficient plasmid transfection in several cell lines (Lehto et al., 2010). The RKR motif is similar as the RXR motif (Fig. 6). As our study shows that both the RLTR (RLT**RKR**GLK) and KLGR (KLG**RKR**TLR) modified PEG-LP are equally efficient in targeting LEC, the possibility that the RKR sequence is responsible for this targeting cannot be completely excluded. There is another possibility, i.e. both peptides contain an RXXR motif. According to CendR theory this RXXR sequence is essential for a tissue penetrating property (Teesalu et al., 2009). As our peptide sequence RLTR (**RLTR**KRGLK) and KLGR (**KLGR**KRTLR) both have the RXXR sequence and supporting CendR theory so there is another possibility that **RLTR** and **KLGR** are the true motifs for these two peptides for targeting LEC (Fig. 6). Both the peptide, RLTR and KTLR, modified LPs appear to have similar targeting abilities for liver EC. However, we were not able to identify the receptor or the key motif responsible for this targeting. Further study will be required to identify the motif or the receptor. LDL receptor, LRP-1, RXR or RXXR motif, which are mentioned in the introduction and discussion, are all possibilities.

5. Conclusion

Liposomes modified with the peptide sequence RLTRKRGLK or its reverse sequence KLGRKRTLR, designed based on the ApoB-100 sequence, accumulated at high levels in liver endothelial cells via some as-yet-unidentified target receptors, and not via non-specific binding with the cell surface. The presence of RXR or RXXR motif in both peptides may explain their similar uptake by liver ECs. The RLTR or KLGR modified liposomes have the potential for use as a carrier system for the delivery of drugs to liver endothelial cells.

Acknowledgements

This study was supported by grants from the Special Education and Research Expenses of the Ministry of Education, Culture, Sports, Science and Technology of Japan. The authors also wish to thank Dr. Milton S. Feather for his helpful advice in writing the English manuscript.

References

Akino, T., Hida, K., Hida, Y., Tsuchiya, K., Freedman, D., Muraki, C., 2009. Cytogenetic abnormalities of tumor-associated endothelial cells in human malignant tumors. Am. J. Pathol. 75, 2657–2667.

Bartsch, M., Weeke-Klimp, A.H., Hoenselaar, E.P., Stuart, M.C., Meijer, D.K., Scherphof, G.L., Kamps, J.A., 2004. Stabilized lipid coated lipoplexes for the delivery of antisense oligonucleotides to liver endothelial cells in vitro and in vivo. J. Drug Target. 12, 613–621.

Brown, M.S., Deuel, T.F., Basu, S.K., Goldstein, J.L., 1978. Inhibition of binding of low density lipoprotein to its cell surface receptors in human fibroblasts by positively charged proteins. J. Supramol. Struct. 8, 223–234.

Dominique, T., Vijay, S., 2010. Intrahepatic angiogenesis and sinusoidal remodeling in chronic liver disease: new targets for the treatment of portal hypertension? J. Hepatol. 53, 976–980.

Du, S.L., Pan, H., Lu, W.Y., Wang, J.W., Wang, J.Y., 2007. Cyclic Arg-Gly-Asp peptide labeled liposomes for targeting drug therapy of hepatic fibrosis in rats. J. Pharmacol. Exp. Ther. 322, 560–568.

Hatakeyama, H., Akita, H., Maruyama, K., Suhara, T., Harashima, H., 2004. Factors governing the in vivo tissue uptake of transferring-coupled polyethylene glycol liposomes in vivo. Int. J. Pharm. 281, 25–33.

Hida, K., Hida, Y., Amin, D.N., Flint, A.F., Panigrahy, D., Mortonet, C.C., 2004. Tumor-associated endothelial cells with cytogeneric abnormalities. Cancer Res. 64, 8249–8255.

Ishiwata, H., Suzuki, N., Ando, S., Kikuchia, H., Kitagawa, T., 2000. Characteristics and biodistribution of cationic liposomes and their DNA complexes. J. Control. Release 69, 139–148.

Kibria, G., Hatakeyama, H., Harashima, H., 2011. A new peptide motif present in the protective antigen of anthrax toxin exerts its efficiency on the cellular uptake of liposomes and applications for a dual-ligand system. Int. J. Pharm. 412, 106–114.

Kmieć, Z., 2001. Cooperation of liver cells in health and disease. Adv. Anat. Embryol. Cell Biol. 161, 1–151.

Lehto, T., Abes, R., Oskolkov, N., Suhorutšenko, J., Copolovici, D.M., 2010. Delivery of nucleic acids with a stearylated (RxR)4 peptide using a non-covalent co-incubation strategy. J. Control. Release 141, 42–51.

Marit, S.N., Rune, B., Christian, A.D., Grete, M.K., Kaare, R.N., Trond, N.B., 1998. Uptake of LDL in parenchymal and non-parenchymal rabbit liver cells in vivo. Biochem. J. 254, 443–448.

Ohga, N., Hida, K., Hida, Y., Muraki, C., Tsuchiya, K., Matsuda, K., 2009. Inhibitory effects of epigallocatechin-3 gallate, a polyphenol in green tea, on tumor-associated endothelial cells and endothelial progenitor cells. Cancer Sci. 100, 1963–1970.

Oie, C.I., Appa, R.S., Hilden, I., Petersen, I., Gruhler, H.H., Smedsrød, A.B., 2011. Rat liver sinusoidal endothelial cells (LSECs) express functional low density lipoprotein receptor related protein-1 (LRP-1). J. Hepatol. 55, 1346–1352.

Puri, A., Loomis, K., Smith, B., Lee, J., Yavlovich, H., Heldman, A.E., 2009. Lipid-based nanoparticles as pharmaceutical drug carriers: from concepts to clinic. Crit. Rev. Ther. Drug Carrier Syst. 26, 523–580.

Ramadori, G., Moriconi, F., Malik, I., Dudas, J., 2008. Physiology and pathophysiology of liver inflammation, damage and repair. J. Physiol. Pharmacol. 59, 107–117.

Rajkumar, C., Gerene, M.D., Gee, W.L., Michael, C.G., Sarah, N.H., David, G., Le, C., 2010. Pathogenesis of the hyperlipidemia of Gram-negative bacterial sepsis may involve pathomorphological changes in liver sinusoidal endothelial cells. Int. J. Infect. Dis. 14, e857–e867.

Teesalu, T., Sugahara, K.N., Kotamraju, V.R., Ruoslahti, E., 2009. C-end rule peptides mediate neuropilin-1-dependent cell, vascular, and tissue penetration. Proc. Natl. Acad. Sci. U.S.A. 106, 16157–16162.

Thomas, E.W., Anders, N., Joachim, H., 1999. Lipoprotein receptors: new roles for ancient proteins. Nat. Cell Biol. 1, 157–162.

Toriyabe, N., Hayashi, Y., Hyodo, M., Harashima, H., 2011. Synthesis and evaluation of stearylated hyaluronic acid for the active delivery of liposomes to liver endothelial cells. Biol. Pharm. Bull. 34, 1084–1089.

Urban, O., German, C., Goran, B., 1993. Binding of a synthetic apolipoprotein B-100 peptide and peptide analogues to chondroitin 6-sulfate: effects of the lipid environment. Biochemistry 32, 1858–1865.

Urban, O., German, C., Eva, H., Karin, C., Goran, E.B., 1997. Possible functional interactions of apolipoprotein B-100 segments that associate with cell proteoglycans and the ApoB/E receptor. Arterioscler. Thromb. Vasc. Biol. 17, 149–152.

ADVANCED HEALTHCARE MATERIALS
www.advhealthmat.de

Materials Views
www.MaterialsViews.com

A Neutral Envelope-Type Nanoparticle Containing pH-Responsive and SS-Cleavable Lipid-Like Material as a Carrier for Plasmid DNA

Hidetaka Akita, Ryohei Ishiba, Hiroto Hatakeyama, Hiroki Tanaka, Yusuke Sato, Kota Tange, Masaya Arai, Kazuhiro Kubo, and Hideyoshi Harashima**

The ultimate demand for gene therapy involves the development of nano-sized particles, which are appropriately designed so as to overcome the multiple biomembrane barriers (i.e., plasma/endosome- and nuclear membranes) to the nuclear delivery of plasmid DNA (pDNA), and to maximize the efficiency of post-nuclear delivery processes (i.e., transcription and translation).[1] Since relatively high concentrations of negatively charged constituents, such as heparan sulfate proteoglycans (HSPGs), are located on the surface of the plasma membrane, many of the previous vectors were designed to carry a high level of positive charges, by the extensive condensation of pDNA with cationic liposomes and polycations under the assumption that cationic charge is a crucial driving force for the first cellular contact with HSPG, and the subsequent cellular uptake process.[2] Meanwhile, quantitative comparisons of intracellular trafficking between cationic non-viral vectors (i.e. lipoplex) and adenovirus revealed that the post-nuclear processes are predominant ones for producing a 2- or 3-magnitude poorer transfection efficiency in non-viral vectors in dividing cells.[3] Further mechanism-based studies revealed that the poor post-nuclear delivery processes can be directly attributed to the inefficiency associated with transcription and translation. This, in turn, can be attributed to the poor release of pDNA from the gene carriers, and to the steric hindrance likely due to electrostatic interactions between mRNA and the cationic component of the gene carrier (i.e., cationic liposomes), respectively.[4] Based on these drawbacks, we focused on the development of a pDNA-encapsulating nanoparticle which was designed to be neutral at physiological (cytoplasmic) pH to avoid mRNA interactions, and to be degradable for the effective release of pDNA in response to the cytoplasmic environment.

Prof. H. Akita,[†] R. Ishiba,[†] Dr. H. Hatakeyama, H. Tanaka, Y. Sato, Prof. H. Harashima
Faculty of Pharmaceutical Sciences
Hokkaido University
Kita 12 Nishi 6, Kita-Ku, Sapporo, Hokkaido, 060-0812, Japan
E-mail: akita@pharm.hokudai.ac.jp; harasima@pharm.hokudai.ac.jp
K. Tange, M. Arai, K. Kubo
NOF Corporation, 3-3 Chidori-cho, Kawasaki-ku, Kawasaki, Kanagawa 210-0865, Japan
[†]H. A. and R. I. equally contributed to this work.

DOI: 10.1002/adhm.201200431

As a fundamental architecture, we used a multifunctional envelope-type nano device (MEND),[5] in which a condensed DNA/polycation complex was coated with lipid envelope (**Figure 1**A). A key molecular component to produce a neutral and degradable envelope is SS-cleavable proton-activated lipid-like material (ssPalm), which has two lipid-like hydrophobic chains ($C_{13}H_{27}$) to form a stable lipid bilayer. This molecule mounts dual sensing motifs that can respond to the intracellular environment; two tertiary amines that function as proton-sponge units, which are positively charged at an acidic pH (endosome/lysosome) for membrane destabilization, and disulfide bonding that can be cleaved in reducing environment (cytosol). Moreover, several prior studies showed that certain kinds of enzymes (i.e., NADH oxidases and protein disulfide-isomerase) have the ability to cleave disulfide bonding on the surface of the cells.[6] Thus, it is possible that the ssPalm might be partially cleaved during the cellular uptake process, and the cleavage product, possessing a proton-receiving tertiary amine (positively charged amine) and a hydrophobic carbon chain might destabilize endosomes by its detergent-like activity. As a control, we synthesized a non-cleavable Palm (ccPalm), in which the ss-cleavable unit was replaced with a covalent carbon linkage. Also, the transfection activity and cellular uptake of the developed MEND was compared with the corresponding values for MENDs prepared with a conventionally cationic lipid (1,2-dioleoyl-3-trimetylammoium propane; DOTAP) and proton-ionizable aminolipid (1,2-Dioleoyl-3-dimethylammonium-Propane; DODAP). While cellular uptake efficiency would be expected to be decreased when the surface of the MEND is neutral, we assumed that these designs, which take the post-nuclear processes into account, might counteract this disadvantage.

For the encapsulation of pDNA, loosely compacted pDNA/protamine core particles were prepared at a nitrogen/phosphate (N/P) ratio of 1.2 in an acidic solution. The particle size of the core particle was 111.4 nm and the zeta potentials were negatively charged (−26.6 mV). Thereafter, the core particles were encapsulated in the lipid envelope by the ethanol dilution method.[7] Palms (ssPalm and ccPalm) and DODAP form vesicular structures with other lipids (1-stearoyl-2-dioleoyl sn-glycero-3-phosphatidylethanolamine; SOPC, cholesterol; Chol and 1-(monomethoxy polyethyleneglycol2000)-2,3-dimyristoylglycerol; PEG_{2000}-DMG) by the stepwise dilution of a lipid solution (99.5% ethanol) with an equal volume of acidic core particle solution (50% ethanol) and further by the addition of an acidic

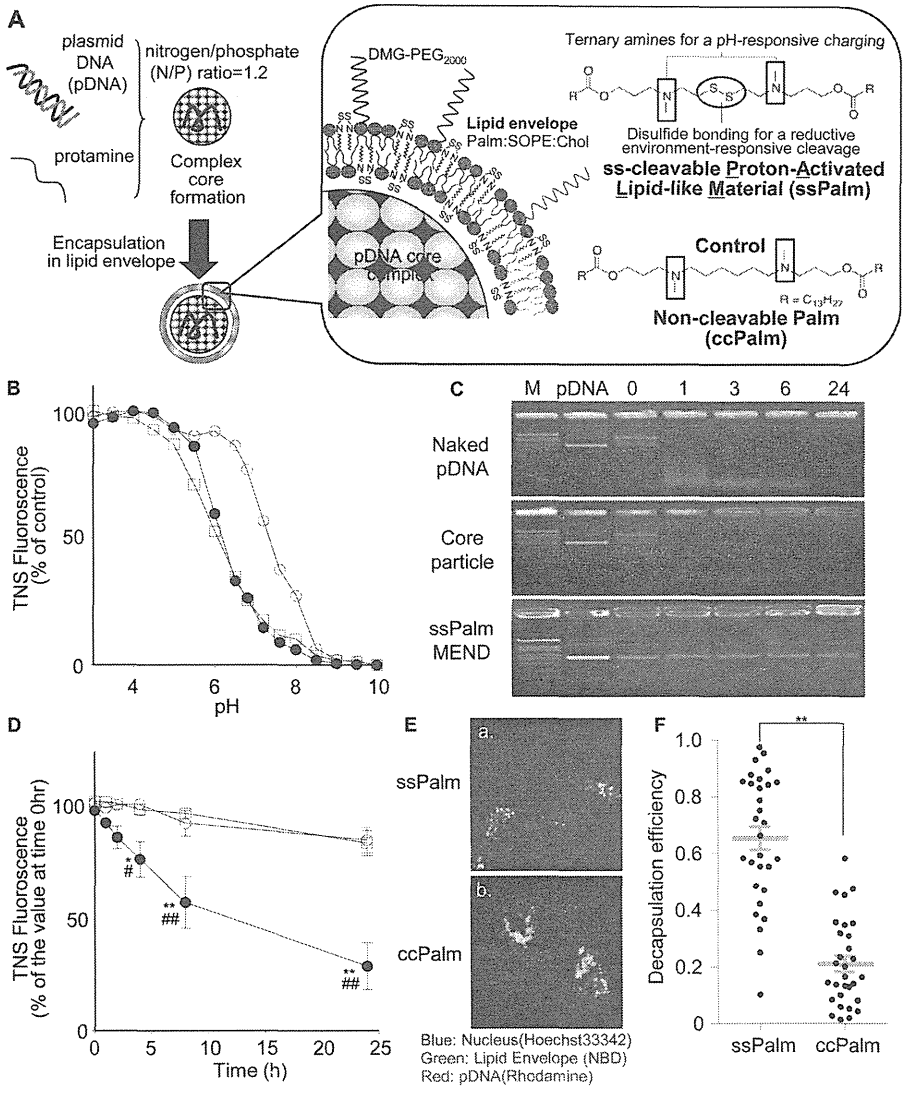

Figure 1. A) Schematic diagram illustrating a $MEND_{ssPalm}$ encapsulating pDNA. ssPalm possesses tertiary amines that cause positive charges to form in response to an acidic environment (endosome/lysosome) and the cleavage of disulfide bonds in a reducing environment (cytosol). B) MENDs prepared with ssPalm ($MEND_{ssPalm}$; closed circle), ccPalm ($MEND_{ccPalm}$; open circle) and DODAP ($MEND_{DODAP}$; open square) were incubated with TNS in various pH to determine an apparent pKa. C) The protection of pDNA against serum nucleases by MENDs. Samples of naked pDNA, pDNA/protamine core particle and $MEND_{ssPalm}$ were added to mouse serum at 1:9 volume ratio at 37 °C for 0–24 h. Aliquots containing 322 ng pDNA of each sample were analyzed by 1.0% agarose gel. D) Time-dependent destabilization in response to the reduction was also investigated by incubating these MENDs with 10 mM DTT for the indicated times. Statistical analyses were performed by Two-way ANOVA followed by Bonferroni's multiple comparison test ($^{*}p < 0.05$ and $^{**}p < 0.01$ against ccPalm, $^{\#}p < 0.05$ and $^{\#\#}p < 0.01$ against DODAP). E) Intracellular decapsulation of pDNA from $MEND_{ssPalm}$ (a) and $MEND_{ccPalm}$ (b) in HT1080 cells at 6 h post-transfection. F) Dissociation efficiencies of $MEND_{ssPalm}$ and $MEND_{ccPalm}$ in 30 individual cells were plotted with mean values (bar) ± S.E. Statistical analyses were performed by non-parametric Mann-Whitney test ($^{**}p < 0.01$).

HEPES buffer (5% ethanol). The resulting MEND particles were concentrated by ultrafiltration, and then diluted with neutral HEPES (pH = 7.4) to the desired concentration. In the encapsulation process, the incorporation of PEG-lipid (>3 mol% of total lipid) is also essential to achieve a small-sized and highly dispersed particle population, presumably because the hydrophilic PEG layer avoids particle-to-particle collisions. Encapsulation efficiencies of pDNA in MENDs were determined as >80% by using gel retardation assay (Supplemental Figure S1).

The size and ξ-potentials of the MENDs used in the present study are summarized in Supplemental Table 1. MENDs prepared by ethanol dilution methods are comparable in size (130–160 nm). The ξ-potentials of MENDs prepared with ssPalm and DODAP ($MEND_{ssPalm}$ and $MEND_{DODAP}$, respectively) were nearly neutral, while that of ccPalm ($MEND_{ccPalm}$) was unexpectedly positive (approximately +10 mV). As another control, we prepared a MEND composed of DOTAP/DOPE/Chol (30:40:30) by the lipid hydration method ($MEND_{DOTAP}$), which is known

ADVANCED HEALTHCARE MATERIALS
www.advhealthmat.de

www.MaterialsViews.com

to exhibit a high gene expression in the presence of serum.[8] This MEND was highly cationic (> +50 mV), derived from the quaternary amines in DOTAP. This MEND also has a relatively larger size and polydispersity index (PDI) compared to particles prepared by the ethanol dilution method.

The apparent pKa values for the ssPalm, ccPalm and DODAP in the lipid bilayer were determined by incorporating a fluorescence probe; potassium 2-(*p*-toluidino)-6-naphthalenesulfonic acid (TNS) into the lipid envelope (Figure 1B). The values for ssPalm and DODAP were comparable (approximately 6.2 and 6.0, respectively). On the other hand, the pKa of ccPalm was approximately 7.3. This data is consistent with the fact that $MEND_{ccPalm}$ particles carry a slight positive charge, while the $MEND_{ssPalm}$ and $MEND_{DODAP}$ are neutral (Supplemental Table 1). The stability of the $MEND_{ssPalm}$ in mouse serum was assessed. Naked DNA, the pDNA/protamine core particle and the $MEND_{ssPalm}$ were incubated in 90% mouse serum for 24 h. After purifying the pDNA, the samples were analyzed by agarose gel electrophoresis (Figure 1C). pDNA encapsulated in the $MEND_{ssPalm}$ was stable for at least 24 h, while naked DNA and pDNA/protamine core particles were rapidly degraded within 1 h. These data strongly indicate that the encapsulation into the lipid envelope provides protection from enzymatic degradation when the encapsulated cargo is in blood circulation. The stability of the lipid envelope under the reductive environment was also evaluated by a TNS assay. The MENDs were incubated in the presence or absence of 10 mM DTT as a reducing reagent for the indicated durations. Thereafter, TNS was incubated with MENDs at pH 4.0, in which most tertiary amines are charged positive regardless of the lipid component (Figure 1B). As shown in Figure 1D, TNS fluorescence was gradually reduced in the case of the $MEND_{ssPalm}$, while those of MENDs prepared with non-cleavable lipids ($MEND_{ccPalm}$ and $MEND_{DODAP}$) remained constant throughout the experiment. Thus, cleavage of the disulfide bonding destabilizes the lipid envelope of $MEND_{ssPalm}$ in response to the reducing environment. However, this reaction occurred slowly over a 24 hr period whereas the DTT-mediated cleavage of disulfide bonding was generally complete within 30 ~ 1 h, at most.[9] In this assay, the reduction in fluorescence can be observed when the quantity of the TNS inserted into the lipid envelope is decreased, and/or the lipid bilayer loses hydrophobicity in parallel with the destabilization of the lipid envelope. In this sense, the parameter determined in this experiment is a hybrid of the efficiency of SS-cleavage and subsequent destabilization of the particle. Therefore, it is plausible that the slow decrease in TNS fluorescence may be rate-limited by the latter process. To investigate the destabilization and resulting decapsulation pDNA in the cell, a double-labeled MEND was prepared, in which the pDNA was labeled with rhodamine and the lipid envelope was labeled with 7-nitrobenz-2-oxa-1,3-diazole (NBD). In the case of the $MEND_{ccPalm}$, pDNA signals were predominantly co-localized with the lipid envelope signals (Figure 1E; b). In contrast, a significant portion of the pDNA signals were detected as non-colocalized forms in the $MEND_{ssPalm}$ (Figure 1E; a), while a major portion of the pDNA remained in the envelope structure at an earlier time (at <10 min after transfection) (Supplemental Figure S2). In fact, the mean decapsulation efficiency in the $MEND_{ssPalm}$ quantified using 30 individual cells was significantly higher than those in the $MEND_{ccPalm}$ (0.65 and 0.21, respectively) even at 6 h after transfection (Figure 1F). These data suggest that the decapsulation efficiency was actually improved after the particles were taken up into the cells, as was intended in the design. Such an earlier intracellular decapsulation of $MEND_{ssPalm}$ in comparison with a DTT-mediated in vitro destabilization (Figure 1D) can be explained by assuming that an association with a variety of the lipid binging proteins or negatively charged mRNAs might trigger destabilization in the cells.

To evaluate the intracellular trafficking of the $MEND_{ssPalm}$, the co-localization of the MENDs with endosomes/lysosomes were observed by confocal laser scanning microscopy (Figure 2A). The $MEND_{ssPalm}$, $MEND_{ccPalm}$ and $MEND_{DODAP}$ were observed as well-dispersed particles (a–c). In contrast, the $MEND_{DOTAP}$ forms large sediments on the bottom of a dish or a cell (d). Thus, the hydrophilic PEG layer might prevent mutual particle-to-particle collision. Among these well-dispersed particles, pDNA signals (pseudo-colored in red) free from co-localization with endosomes/lysosomes (green) were commonly observed in the case of the $MEND_{ssPalm}$ (Figure 2A;a), especially in comparison with $MEND_{DODAP}$ (Figure 2A;c). Further quantification of the co-localization of the pDNA with endosome/lysosome using 30 cells revealed that the endosomal escape efficiency can be ranked as follows: $MEND_{ssPalm} > MEND_{ccPalm} > MEND_{DODAP}$ (Figure 2B). Thus, the use of ssPalm has clear advantages in terms of the endosomal escape process, compared to DODAP or ccPalm.

To investigate the mechanism responsible for the efficient endosomal escape of $MEND_{ssPalm}$, the impact of endosomal acidification on transgene expression was first addressed. As shown in Figure 2C, the gene expression level for the $MEND_{ssPalm}$ and $MEND_{DODAP}$ was decreased in the presence of bafilomycin A1, a specific inhibitor of vacuolar-type H^+-ATPase. In contrast, the gene expression of the $MEND_{ccPalm}$ and $MEND_{DOTAP}$ were not inhibited, probably because they are positively charged regardless of the pH of their environment. Similar results were also observed when we used NH_4Cl, another type of blocker of endosomal acidification (Supplemental Figure S3). Thus, pH-activated positive charging is prerequisite for the destabilization of endosomes in the $MEND_{ssPalm}$ and $MEND_{DODAP}$, and this occurs by triggering the electrostatic interaction between MEND particles to the endosomal membrane. In addition, the 'proton sponge mechanism' derived from the proton-accepting secondary amines is one of the possible mechanisms for explaining endosomal destabilization as was shown in the case of polyethyleneimine (PEI).[10] The higher proton-buffering capacity in the $MEND_{ssPalm}$ might result in the fact that its more endosomal escape efficiency is greater than that of $MEND_{ccPalm}$.

However, the pH-dependent positive charging and/or "proton sponge effect" cannot explain the issue of why the $MEND_{ssPalm}$ is able to escape from the endosome more effectively than $MEND_{DODAP}$, given the fact that these MENDs have similar apparent pKa values. To address this question, we evaluated the destabilization of the cell membrane more directly by a hemolysis assay (Figure 2D). Liposomes composed of ssPalm/DODAP:SOPE:Chol (30:40:30) plus PEG_{2000}-DMG (LP_{ssPalm} and LP_{DODAP}) were incubated with erythrocytes at various pH values. As described above, a part of the disulfide bonding in

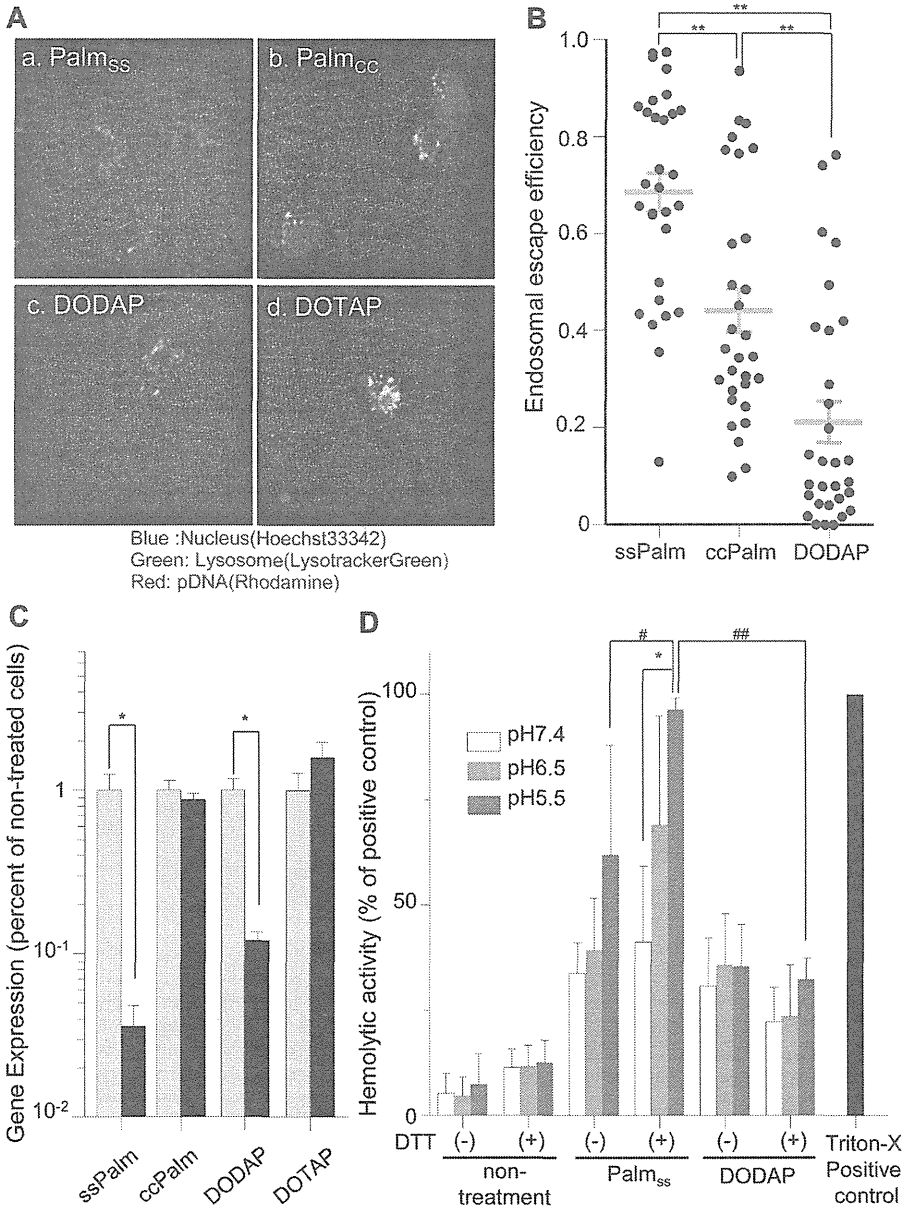

Figure 2. A) Rhodamine-labeled pDNA was encapsulated in MEND$_{ssPalm}$ (a), MEND$_{ccPalm}$ (b), MEND$_{DODAP}$ (c) and MEND$_{DOTAP}$ (d), and then were transfected to the HT1080 cells for 3 h. B) Endosome escape efficiencies of the MEND$_{ssPalm}$ and MEND$_{ccPalm}$ and MEND$_{DODAP}$ in 30 individual cells were plotted with mean values (bar) ± S.E. Statistical analyses were performed by non-parametric Kruskal-Wallis test followed by Dunn's multiple comparison test (**; $p < 0.01$). C) MENDs were transfected to the HT1080 cells that had been pretreated with bafilomycin A1. The transfection activities of MEND were expressed as the relative mean values of those obtained in the absence of bafilomycin A1. Statistical analyses were performed by Two-way ANOVA followed by Bonferroni's multi-comparison test (*;$p < 0.05$). C) Erythrocytes were incubated with LP$_{ssPalm}$ and LP$_{DODAP}$ at various pH in the presence or absence of DTT for 30 min. The absorbance of the hemoglobin that had leaked into the supernatant was measured. The values were represented as relative values of the positive control, obtained by triton X-100 treatment. Statistical analyses were performed by One-way ANOVA followed by Bonferroni's multi-comparison test (*;$p < 0.05$), or One-way ANOVA followed by Unpaired T-test (#; $p < 0.05$, ##;$p < 0.01$).

ssPalm on the plasma membrane might be cleaved.[6] Thus, we also monitored hemolysis activity in the presence of DTT as an artificial cleavage inducer of ssPalm to investigate the potential role of the SS-cleaved product in the membrane destabilization process. At physiological pH, the hemolysis activity of LP$_{ssPalm}$ was marginal and also comparable to that of LP$_{DODAP}$. However, the hemolysis activities of the LP$_{ssPalm}$ tended to increase in response to the acidic environment, especially in the presence of DTT. In contrast, hemolysis activity was not altered regardless of the acidification or DTT treatment in the case of

ADVANCED HEALTHCARE MATERIALS
www.advhealthmat.de

Materials Views
www.MaterialsViews.com

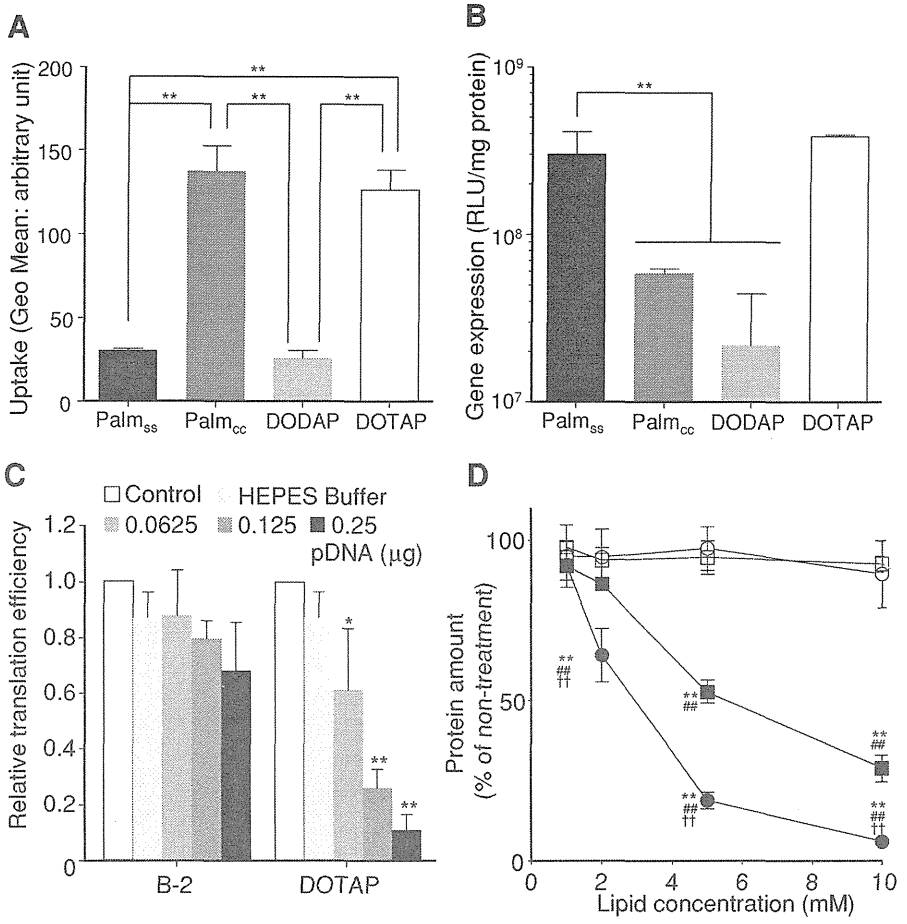

Figure 3. A) Cellular uptake of NBD-labeled $MEND_{ssPalm}$, $MEND_{ccPalm}$, $MEND_{DODAP}$ and $MEND_{DOTAP}$ were quantified by FACS, and the geo mean fluorescence was then calculated. B) Transfection activities of MENDs in HT1080 cells were evaluated at for 24 h post-transfection. Statistical analyses were performed by One-way ANOVA followed by Bonferroni's multi-comparison test (**;$p < 0.01$). C) mRNA encoding luciferase was subjected to in vitro translation in the presence $MEND_{ssPalm}$ and $MEND_{DOTAP}$ at the indicated amount of pDNA. Statistical analyses were performed by Two-way ANOVA followed by Bonferroni's multi-comparison test (*;$p < 0.05$,**;$p < 0.01$ against HEPES buffer). D) Cytotoxicities of MENDs, in terms of the amount of remaining protein amount in each tested well were evaluated by transfection at various concentrations. Open circles, closed circles, open squares and closed squares represent $MEND_{ssPalm}$, $MEND_{ccPalm}$, $MEND_{DODAP}$, $MEND_{DOTAP}$, respectively. Statistical analyses were performed by Two-way ANOVA followed by Bonferroni's multiple comparison test (**; $p<0.01$ against ssPalm, ##; $p < 0.01$ against DODAP and ††; $p < 0.01$ against DOTAP).

the LP_{DODAP}. Thus, along with a positive charge, the structure of ssPalm is an important characteristic for efficient endosomal escape.

As a functional analysis, we first compared the cellular uptake of MENDs to HT1080 cells using fluorescence-activated cell sorting (Figure 3A). Since the surface positive charge is a driving force for the cellular binding of MENDs, the cellular uptake of cationic MENDs ($MEND_{ccPalm}$ and $MEND_{DOTAP}$) would be expected to be significantly higher than neutral MENDs ($MEND_{ssPalm}$ and $MEND_{DODAP}$). In contrast, the rank order of trans-gene expression was $MEND_{ssPalm} > MEND_{ccPalm} > MEND_{DODAP}$ (Figure 3B). Of note, the gene expression of the $MEND_{ssPalm}$ was approximately 20-fold higher than that of the $MEND_{DODAP}$. Moreover, the most significant finding was that the expression level of the $MEND_{ssPalm}$ was comparable to that for the $MEND_{DOTAP}$. This indicates that the drawback to the use of a neutral $MEND_{ssPalm}$: less cellular uptake, was counteracted by the efficient intracellular processing.

In our evaluations of the endosomal escape processes, the $MEND_{DOTAP}$ escapes from endosomes as efficient as $MEND_{ssPalm}$ (Figure 2A). Furthermore, in the present study, pDNA appears to enter the nucleus at the mitosis phase when the nuclear membrane structure is temporarily diminished. Thus, higher efficiency of the $MEND_{ssPalm}$ in the intracellular processes can be attributed to post-nuclear processes, due to the active decapsulation of pDNA (Figure 1E and 1F) and less electrostatic interaction with mRNA as was intended in the original design. This hypothesis is supported by the fact that $MEND_{ssPalm}$ marginally inhibited the in vitro translation of the mRNA, while a drastic loss of the reaction was observed in the cationic $MEND_{DOTAP}$ (Figure 3C).

Since safety is a minimum requirement for the future in vivo use of gene carriers, we finally evaluated the MENDs for cytotoxicity (Figure 3D). On the x-axis, the dose was represented as the total lipid concentration. The minimum dose (1.5 mM) is the generally used concentration for in vitro gene transfection (corresponding to the 0.4 μg/mL of pDNA). The Y-axis represents the cytotoxicity of the MEND in terms of the amount of protein after a 24 h-transfection. In the case of the $MEND_{ccPalm}$ and $MEND_{DOTAP}$, the amount of protein was drastically decreased depending on the dose increase. Even in these higher dose transfections, the amount of protein was never decreased in the $MEND_{ssPalm}$ and $MEND_{DODAP}$. The lower toxicity of the $MEND_{ssPalm}$ in comparison with $MEND_{ccPalm}$ can be explained by its efficient biodegradation in the cells. Previous studies showed that cationic lipids with biodegradable characteristics[11] (i.e., cationic cholesterol linked with carbamate ester bonding[12]) are less toxic. Furthermore, in our molecular design, the number of amine(s) per molecule decreased from 2 to 1 by the cleavage of disulfide bonding. Since cross-linkage of a low-molecular PEI with a disulfide linkage confers lower toxicities with superior transfection efficacies in comparison with a high molecular PEI,[13] depolymerization of the cationic units concomitant with biodegradation might be a key factor in terms of avoiding cytotoxicity.

In summary, we report on the successful development of a pDNA carrier, which is designed to maximize the post-nuclear delivery processes (transcription and translation) by excluding surface positive charges and promoting biodegradability. As a result, a gene transfection activity comparable to that of a conventional cationic MEND was achieved in the presence of serum with much a smaller amount of cellular uptake. Also, cytotoxicity was extremely low, presumably due to its biodegradable nature. As a future issue, the poor cellular uptake of neutral particles can be conquered by surface modification with cell-targeting ligands. Finally, the exclusion of cationic charge is also advantageous to avoid undesirable accumulation in the lung,[14] and to prolong the systemic circulation after intravenous administration.[15] This carrier will be a promising carrier for in vivo use in the future.

Experimental Section

Full methods for the synthesis, preparation/characterization of nanoparticle and functional analysis are described in the Supporting Information.

Supporting Information

Supporting Information is available from the Wiley Online Library or from the author.

Acknowledgements

This work is supported by Funding Program for Next Generation World-Leading Researchers (NEXT Program), and partially by Grant-in-Aid for Scientific Research (S) from the Ministry of Education, Culture, Sports, Science and Technology (MEXT) of Japan. Authors also receive funding from NOF Corporation. H.A. is also supported by the Asahi Glass Foundation. The authors would also like to thank Dr. M. S. Feather for his helpful advice in writing the English manuscript. H.A. and R.I. contributed equally to this work.

Received: November 21, 2012
Published online: February 6, 2013

[1] a) H. Akita, H. Harashima, *Expert Opin. Drug Delivery* **2008**, *5*, 847; b) H. Kamiya, H. Akita, H. Harashima, *Drug Discovery Today* **2003**, *8*, 990.
[2] a) C. Marty, C. Meylan, H. Schott, K. Ballmer-Hofer, R. A. Schwendener, *Cell Mol Life Sci.* **2004**, *61*, 1785; b) K. A. Mislick, J. D. Baldeschwieler, *Proc. Natl. Acad. Sci. USA* **1996**, *93*, 12349; c) L. C. Mounkes, W. Zhong, G. Cipres-Palacin, T. D. Heath, R. J. Debs, *J. Biol. Chem.* **1998**, *273*, 26164.
[3] a) S. Hama, H. Akita, R. Ito, H. Mizuguchi, T. Hayakawa, H. Harashima, *Mol. Ther.* **2006**, *13*, 786; b) C. M. Varga, N. C. Tedford, M. Thomas, A. M. Klibanov, L. G. Griffith, D. A. Lauffenburger, *Gene Ther.* **2005**, *12*, 1023.
[4] S. Hama, H. Akita, S. Iida, H. Mizuguchi, H. Harashima, *Nucleic Acids Res.* **2007**, *35*, 1533.
[5] a) K. Kogure, H. Akita, H. Harashima, *J. Controlled Release* **2007**, *122*, 246; b) K. Kogure, H. Akita, Y. Yamada, H. Harashima, *Adv. Drug Delivery Rev.* **2008**, *60*, 559.
[6] a) E. P. Feener, W. C. Shen, H. J. Ryser, *J Biol Chem* **1990**, *265*, 18780; b) R. Mandel, H. J. Ryser, F. Ghani, M. Wu, D. Peak, *Proc. Natl. Acad. Sci. USA* **1993**, *90*, 4112; c) D. J. Morre, D. M. Morre, *Free Radical Res.* **2003**, *37*, 795.
[7] L. B. Jeffs, L. R. Palmer, E. G. Ambegia, C. Giesbrecht, S. Ewanick, I. MacLachlan, *Pharm Res.* **2005**, *22*, 362.
[8] H. Hatakeyama, H. Akita, K. Kogure, M. Oishi, Y. Nagasaki, Y. Kihira, M. Ueno, H. Kobayashi, H. Kikuchi, H. Harashima, *Gene Ther.* **2007**, *14*, 68.
[9] M. A. Gosselin, W. Guo, R. J. Lee, *Bioconjug. Chem.* **2001**, *12*, 989.
[10] a) J. P. Behr, *Chimia* **1997**, *51*, 34; b) A. E. Nel, L. Madler, D. Velegol, T. Xia, E. M. Hoek, P. Somasundaran, F. Klaessig, V. Castranova, M. Thompson, *Nat. Mater.* **2009**, *8*, 543.
[11] R. Leventis, J. R. Silvius, *Biochim. Biophys. Acta* **1990**, *1023*, 124.
[12] J. S. Choi, E. J. Lee, H. S. Jang, J. S. Park, *Bioconjug. Chem.* **2001**, *12*, 108.
[13] M. Breunig, U. Lungwitz, R. Liebl, A. Goepferich, *Proc. Natl. Acad. Sci. USA* **2007**, *104*, 14454.
[14] S. Fumoto, S. Kawakami, K. Shigeta, Y. Higuchi, F. Yamashita, M. Hashida, *J. Pharmacol. Exp. Ther.* **2005**, *315*, 484.
[15] S. C. Semple, S. K. Klimuk, T. O. Harasym, N. Dos Santos, S. M. Ansell, K. F. Wong, N. Maurer, H. Stark, P. R. Cullis, M. J. Hope, P. Scherrer, *Biochim. Biophys. Acta* **2001**, *1510*, 152.

Published online 11 September 2013 *Nucleic Acids Research, 2013, Vol. 41, No. 22* ***10659–10667***
doi:10.1093/nar/gkt823

In vitro optimization of 2′-OMe-4′-thioribonucleoside–modified anti-microRNA oligonucleotides and its targeting delivery to mouse liver using a liposomal nanoparticle

Mayumi Takahashi[1], Naoki Yamada[1], Hiroto Hatakeyama[1], Manami Murata[1], Yusuke Sato[1], Noriaki Minakawa[2], Hideyoshi Harashima[1] and Akira Matsuda[1,*]

[1]Faculty of Pharmaceutical Sciences, Hokkaido University, Kita-12, Nishi-6, Kita-ku, Sapporo 060-0812, Japan and [2]Graduate School of Pharmaceutical Sciences, The University of Tokushima, Shomachi 1-78-1, Tokushima 770-8505, Japan

Received July 14, 2013; Revised August 20, 2013; Accepted August 21, 2013

ABSTRACT

MicroRNAs (miRNAs) are small noncoding RNAs that regulate gene expression post-transcriptionally. Previous studies, which characterized miRNA function, revealed their involvement in fundamental biological processes. Importantly, miRNA expression is deregulated in many human diseases. Specific inhibition of miRNAs using chemically modified anti-miRNA oligonucleotides (AMOs) can be a potential therapeutic strategy for diseases in which a specific miRNA is overexpressed. 2′-O-Methyl (2′-OMe)-4′-thioRNA is a hybrid type of chemically modified oligonucleotide, exhibiting high binding affinity to complementary RNAs and high resistance to nuclease degradation. Here, we evaluate 2′-OMe-4′-thioribonucleosides for chemical modification on AMOs. Optimization of the modification pattern using a variety of chemically modified AMOs that are perfectly complementary to mature miR-21 revealed that the uniformly 2′-OMe-4′-thioribonucleoside–modified AMO was most potent. Further investigation showed that phosphorothioate modification contributed to long-term miR-122 inhibition by the 2′-OMe-4′-thioribonucleoside–modified AMO. Moreover, systemically administrated AMOs to mouse using a liposomal delivery system, YSK05-MEND, showed delivery to the liver and efficient inhibition of miR-122 activity at a low dose *in vivo*.

INTRODUCTION

MicroRNAs (miRNAs) are a class of endogenously expressed small noncoding RNAs (18∼25 nt), which regulate gene expression post-transcriptionally. In animals, single-stranded mature miRNAs hybridize to the 3′ untranslated region (3′UTR) of the target mRNA through complete base paring with positions 2–8 of the miRNA, known as the seed region. Binding on the seed region nucleates miRNA–mRNA association, and causes translational inhibition or mRNA degradation (1,2). Because complementarity of the seed region consists of only 7 nt, a single miRNA may regulate multiple genes, and a single mRNA can be modulated by several different miRNAs (3–5). To date, >1000 miRNAs have been identified in humans and regulate up to 60% of protein coding genes (6,7). MiRNAs are implicated in important functions in the biological process, including cell differentiation, proliferation, development, metabolism and apoptosis. Furthermore, up- or downregulation of miRNA expression is correlated with a variety of human diseases such as cancer, viral infection and cardiovascular disorders (8). Thus, regulation of specific miRNA function is a promising therapeutic strategy for treatment of such diseases.

Among the approaches to modulate the function of miRNAs, anti-miRNA oligonucleotide (AMO)-based inhibition has been most widely used not only to exploit the biological function of miRNAs but also as candidates for therapeutic agents (9). To develop oligonucleotide (ON)-based therapeutic strategies, there are several issues to overcome, namely poor stability of ONs in biological fluids, weak binding affinity to target RNA, poor cellular uptake and unfavorable immunostimulatory activity. Thus far, a wide variety of chemically modified ONs have been developed to date, including 2′-*O*-methyl (2′-OMe) (10–13), 2′-*O*-methoxyethyl (14) and locked nucleic acid (LNA) to overcome these disadvantages (15–17). These chemical modifications have successfully been applied to an antisense technology as well as

*To whom correspondence should be addressed. Tel: +81 11 706 3228; Fax: +81 11 706 4980; Email: matuda@pharm.hokudai.ac.jp

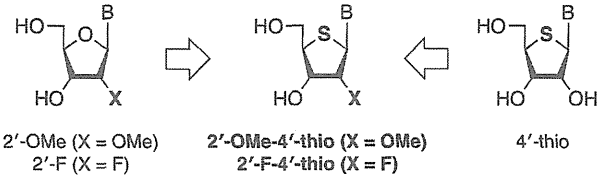

Figure 1. Structure of 2′-modified-4′-thioribonucleoside.

ON-based therapeutic technologies (e.g. siRNAs, aptamers, ribozymes). Two successful reports of 2′-OMe–modified AMOs were reported in 2004 (18,19), lending credence to the idea of using chemically modified AMOs. Furthermore, considerable efforts in optimization have been dedicated to develop AMOs as a new therapeutic agent, and several chemically modified AMOs are currently undergoing clinical trials (20). Therefore, further optimization of chemical modifications for AMO-based miRNA suppression will continue to improve this therapeutic approach.

We developed a novel chemically modified ON, 2′-OMe-4′-thioRNA (21) (Figure 1), which can be considered a hybrid chemical modification based on 2′-OMe RNA (13) and 4′-thioRNA (22–28). In our previous study, we reported the development of 2′-OMe-4′-thioribonucleoside–modified siRNA (29). Optimization of both the number and position of modification by 2′-OMe-4′-thioribonucleoside afforded modified siRNAs with more potent and persistent RNAi activity. In addition, investigation of the duration of RNAi activity resulted in long-lasting gene silencing *in vitro* owing to the improved intracellular stability of 2′-OMe-4′-thioribonucleoside–modified siRNA. Like many other chemically modified ONs that can successfully be applied to AMO as well as siRNA, we expected that 2′-OMe-4′-thioribonucleoside modification acts as a promising AMO. Therefore, we set out to evaluate the utility of 2′-OMe-4′-thioribonucleoside for chemical modification on AMOs. In this study, we investigated the modification pattern of AMOs by 2′-OMe-4-thioribonucleoside in terms of potency and duration of activity in two kinds of target miRNA (miR-21 and miR-122) *in vitro*. Moreover, systemically administrated AMOs to mouse liver using a liposomal delivery system, a multifunctional envelope-type nano device (MEND) with a pH-sensitive cationic lipid, YSK05 (YSK05-MEND) (30), showed efficient inhibition of miR-122 activity at a low dose *in vivo*, implicating potential use of 2′-OMe-4′-thioribonucleoside–modified AMO in nucleic acid therapy.

MATERIALS AND METHODS

Oligonucleotides

The chemically modified AMOs used in this study were synthesized on an Applied Biosystem 3400 DNA synthesizer according to our previous report (21). Thus, support bound chemically modified AMOs were synthesized using the corresponding phosphoramidite units at a 1.0 μmol scale following the standard procedure described for oligoribonucleotides. Each of the phosphoramidite units was used at a concentration of 0.1 M in dry acetonitrile, and the coupling time was extended to 10 min for each step. AMOs with phosphorothioate (PS) backbone were achieved by oxidation with 3*H*-1,2-benzodithiol-3-one-1,1-dioxide (Beaucage reagent) during ON synthesis. After completion of the synthesis, the CPG support was treated with concentrated NH_4OH or NH_4OH/EtOH (3:1) at 55°C for 16 h. In the case of CPG supports containing either 2′-F or 2′-F-4′-thioribonucleoside modification, these were treated with methanolic ammonia (saturated at 0°C) at room temperature for 24 h. Then, the support was filtered off. The filtrate was concentrated and the ON protected by a DMTr group at the 5′-end was chromatographed on a C-18 silica gel column with a linear gradient of acetonitrile (from 5 to 40%) in 0.1 N TEAA buffer (pH 7.0). The fractions containing the full-length ON were combined and concentrated. The residue was treated with aqueous acetic acid (70%) for 20 min at room temperature. The solution was concentrated and the residue was purified on reversed-phase high performance liquid chromatography, using a J'sphere ODS-M80 column (4.6 × 150 mm, YMC) with a linear gradient of acetonitrile (from 10 to 40%) in 0.1 N TEAA buffer (pH 7.0). The structures of each RNA were confirmed by measurement of MALDI-TOF/MASS spectrometry on Ultraflex TOF/TOF (Buruker Daltonics). The analytical data of synthetic AMOs are summarized in Supplementary Table S1.

T_m measurement

Thermally induced transitions were monitored at 260 nm on a Beckman DU 650 spectrophotometer. Samples were prepared as follows: AMO and target miRNA (3 μM each) were mixed in a phosphate buffer (10 mM, pH 7.0) containing 0.1 mM EDTA and 1 mM NaCl, heated at 90°C for 5 min, cooled gradually to room temperature and used in thermal denaturation studies. The sample temperature was increased 0.5°C/min.

Cell culture

HeLa cells and Huh-7 cells were cultured at 37°C under 5% CO_2 in Dulbecco's modified Eagle's medium (DMEM, Gibco) supplemented with 10% fetal bovine serum (FBS, Thermo Fisher Scientific), 100 units ml^{-1} penicillin, 100 μg ml^{-1} streptomycin, respectively. Cells were regularly passaged to maintain exponential growth.

Construction of miRNA reporter plasmids and luciferase reporter assay

The miRNA reporter plasmids were generated by cloning the synthetic 5′-phosphorylated ONs corresponding to tandem perfect-match target sited for human miR-21 or miR-122 into the 3′UTR of firefly luciferase gene (luc2) in the pmirGLO Vector (Promega). HeLa cells or Huh-7 cells were plated into 96-well plates, at 10 000 cells/well in DMEM supplemented with 10% FBS, 100 units ml^{-1} penicillin, 100 μg ml^{-1} streptmycin. After 24 h of plating, reporter plasmid and AMOs were co-transfected into the cells in triplicate using Lipofectamine™ 2000